Journal of Scientific Computing (2022) 93:28
https://doi.org/10.1007/s10915-022-01974-w

A Lowest-Degree Conservative Finite Element Scheme for Incompressible Stokes Problems on General Triangulations

Wenjia Liu[1,2] · **Shuo Zhang**[1,2]

Received: 23 January 2022 / Revised: 11 July 2022 / Accepted: 4 August 2022 /
Published online: 7 September 2022
© The Author(s), under exclusive licence to Springer Science+Business Media, LLC, part of Springer Nature 2022

Abstract
In this study, we investigate how low the degree of polynomials can be to construct a stable conservative pair for incompressible Stokes problems that works on general triangulations. We propose a finite element pair that uses a slightly enriched piecewise linear polynomial space for velocity and piecewise constant space for pressure. The pair is illustrated to be a lowest-degree stable conservative pair for Stokes problems on general triangulations.

Keywords Incompressible stokes equations · Inf-sup condition · Conservative scheme · Pressure-robust discretization · Lowest degree

Mathematics Subject Classification 65N12 · 65N15 · 65N22 · 65N30 · 76D05

1 Introduction

For the Stokes problem, if a stable finite element pair can inherit mass conservation, the approximation of the velocity can be independent of the pressure, and the method does not suffer from the locking effect with respect to a high Reynolds number (cf., e.g., [6]). Over the past decade, conservative schemes have been recognized more clearly as *pressure robustness* and widely studied and surveyed in, for example, [13, 15, 22, 29]. This conservation is also connected to other key features such as "viscosity-independence" [33] and "gradient-robustness" [23] for numerical schemes. Conservative schemes are also significant in nonlinear mechanics [4, 5] and magnetohydrodynamics [18–20]. The construction of conservative schemes has thus been drawing wide interests.

✉ Shuo Zhang
szhang@lsec.cc.ac.cn

Wenjia Liu
wjliu@lsec.cc.ac.cn

1 LSEC, Institute of Computational Mathematics and Scientific/Engineering Computing, Academy of Mathematics and Systems Science, Chinese Academy of Sciences, Beijing 100190, People's Republic of China

2 University of Chinese Academy of Sciences, Beijing 100049, People's Republic of China

Various conservative finite element pairs have been designed for the Stokes problem. Conforming examples include conforming elements designed for special meshes, such as $\boldsymbol{P}_k$–P_{k-1} triangular elements for $k \geq 4$ on singular-vertex-free meshes [30], smaller k constructed on composite grids [3, 28, 30, 36, 41], and the pairs given in [12, 15], which work for general triangulations and with extra smoothness requirements. An alternative method is to use $\boldsymbol{H}(\text{div})$-conforming but $\boldsymbol{H}^1$-nonconforming space for the velocity. A systematic approach for finite element methods is to add bubble-like functions onto $\boldsymbol{H}(\text{div})$ finite element spaces for tangential weak continuity for the velocity. Examples along this line can be found in [14, 25, 32] and [35]. Generally, to construct a conservative pair that works on general triangulations without special structures, cubic and higher-degree polynomials are used for the velocity field.

Recently, a new $\boldsymbol{P}_2$–P_1 finite element pair was proposed on general triangulations [37]; for the velocity field, this pair uses piecewise quadratic $\boldsymbol{H}(\text{div})$ functions with enhanced tangential continuity in addition to using discontinuous piecewise linear functions for pressure. The pair is stable and immediately strictly conservative on general triangulations, and is of the lowest degree ever known. As the tangential component of the velocity function is continuous only in the average sense, the convergence rate of the pair is proved to be of $\mathscr{O}(h)$ order. However, due to its strict conservativeness on general triangulations, it plays superior to some $\mathscr{O}(h^2)$ schemes numerically in robustness with respect to triangulations and with respect to small parameters. As pointed out in [37], this $\boldsymbol{P}_2$–P_1 pair can be viewed as a smoothened reduction from the famous second-order Brezzi–Douglas–Marini pair, and this idea can be applied to other $\boldsymbol{H}(\text{div})$ pairs so that the degrees of finite element pairs may be reduced further.

In this work, we study how low the degree of polynomials can be to construct a stable conservative pair that works on general triangulations. We begin with the reduction of the second-order Brezzi–Douglas–Fortin–Marini(BDFM) element pair to construct an auxiliary finite element pair $\boldsymbol{V}_{h0}^{\text{sBDFM}}$–$\mathbb{P}_{h0}^1$ (with $\mathscr{O}(h)$ convergence rate), and then a further reduction of the $\boldsymbol{V}_{h0}^{\text{sBDFM}}$–$\mathbb{P}_{h0}^1$ pair leads to a $\boldsymbol{V}_{h0}^{\text{el}}$–$\mathbb{P}_{h0}^0$ pair. The finally proposed pair, as the centerpiece of this study, uses a slightly enriched piecewise linear polynomial space for the velocity and piecewise constant for the pressure, and is stable and conservative. A further reduction of this pair leads to a $\boldsymbol{P}_1$–P_0 pair, which is constructed naturally but not stable on general triangulations. Accordingly, we find that the newly designed $\boldsymbol{V}_{h0}^{\text{el}}$–$\mathbb{P}_{h0}^0$ pair is of a lowest-degree conservative pair. We remark that the $\boldsymbol{V}_{h0}^{\text{el}}$–$\mathbb{P}_{h0}^0$ pair is of the type "nonconforming spline" and cannot be represented by Ciarlet's triple. However, the velocity space does admit a set of basis functions with local supports, which are clearly stated in Sect. 5. This makes the pair embedded in the standard framework for programming.

The technical ingredients of this study are twofold. One is to determine the locally supported basis functions of $\boldsymbol{V}_{h0}^{\text{el}}$. The supports are considerably different from those of existing finite elements. However, the explicit formulations of the basis functions make the scheme easy to implement. Another ingredient is to prove the stability of the pair (specifically the inf-sup condition), where we mainly utilize a two-step argument. We first prove the stability of the auxiliary pair $\boldsymbol{V}_{h0}^{\text{sBDFM}}$–$\mathbb{P}_{h0}^1$, and then the stability of the pair $\boldsymbol{V}_{h0}^{\text{el}}$–$\mathbb{P}_{h0}^0$, which is a sub-pair of $\boldsymbol{V}_{h0}^{\text{sBDFM}}$–$\mathbb{P}_{h0}^1$, is proved simply by inheriting the stability of $\boldsymbol{V}_{h0}^{\text{sBDFM}}$–$\mathbb{P}_{h0}^1$. This "reduce-and-inherit" procedure can be found in [46, 47], where some low-degree optimal schemes were designed for other problems. Furthermore, for the velocity space of the auxiliary pair $\boldsymbol{V}_{h0}^{\text{sBDFM}}$–$\mathbb{P}_{h0}^1$, all the degrees of freedom are located on the edges of the triangulation, and it is thus impossible to construct a commutative nodal interpolator with respect to a non-constant pressure space. We adopt Stenberg's macroelement technique [31]. Unlike in the general macroelement argument, on every macroelement, the surjection property of the divergence operator is confirmed by figuring out the kernel space. This technique used to be applied in [38] to show the stability of the Stokes finite element pair. It is natural to generalize all these technical ingredients to other applications.

As a structure of the discretized Stokes complex is given on local macroelements, similar to the study of conservative pairs in [12, 15] and the study of biharmonic finite elements in [11, 39, 45, 46], the proposed global space is embedded in a discretized Stokes complex on the whole triangulation. This global Stokes complex is established in Sect. 4 with a new finite element scheme constructed for the biharmonic equation.

Finally, there have been various schemes constructed for the Stokes problem in the category of discontinuous Galerkin (DG) methods, weak Galerkin (WG) methods, and virtual element methods (VEMs), where extra stabilizations are generally used. They can be found in various studies, such as in [9, 10, 24, 27, 34, 48]. In the present study, we do not discuss such methods in depth and instead focus on methods without stabilization terms.

The rest of the paper is organized as follows. In the remainder of this section, we present some standard notations. Some preliminaries on finite elements are collected in Sect. 2. In Sect. 3, a smoothened BDFM(sBDFM) element and an auxiliary stable conservative pair $\boldsymbol{V}_{h0}^{\mathrm{sBDFM}}$–$\mathbb{P}_{h0}^1$ are established. In Sect. 4, a low-degree continuous nonconforming scheme for the biharmonic equation is presented, together with a discretized Stokes complex. In Sect. 5, a lower-degree stable conservative pair $\boldsymbol{V}_{h0}^{\mathrm{el}}$–$\mathbb{P}_{h0}^0$ is constructed. In Sect. 6, some numerical experiments are reported to demonstrate the effect of the schemes given in the present paper. In Sect. 7, some concluding remarks are given. Finally, it is verified numerically in Appendix A that the most natural $\boldsymbol{P}_1$–P_0 pair, generated by the patch test, is not stable on general shape-regular triangulations. This illustrates that the $\boldsymbol{V}_{h0}^{\mathrm{el}}$–$\mathbb{P}_{h0}^0$ pair is a lowest-degree conservative stable pair on general triangulations.

1.1 Notations

In this paper, we use Ω to denote a simply connected polygonal domain. We use ∇, curl, div, rot, and ∇^2 to denote the gradient operator, curl operator, divergence operator, rot operator, and Hessian operator, respectively. Specifically, curl $v(x, y) = (\frac{\partial v}{\partial y}, -\frac{\partial v}{\partial x})$ and rot $(v_1, v_2) = \frac{\partial v_1}{\partial y} - \frac{\partial v_2}{\partial x}$. Generally, we use $H^1(\Omega)$, $H_0^1(\Omega)$, $H^2(\Omega)$, $H_0^2(\Omega)$, $\boldsymbol{H}(\mathrm{div}, \Omega)$, $\boldsymbol{H}_0(\mathrm{div}, \Omega)$, $H(\mathrm{rot}, \Omega)$, $H_0(\mathrm{rot}, \Omega)$, and $L^2(\Omega)$ to denote certain Sobolev spaces, and denote $L_0^2(\Omega) := \{w \in L^2(\Omega) : \int_\Omega w dx = 0\}$, $\boldsymbol{H}_0^1(\Omega) := (H_0^1(\Omega))^2$. A space written in boldface denotes a two-vector valued analogue of the corresponding scalar space, and naturally, a function written in boldface denotes a two-vector valued analogue of the corresponding scalar function. We use $(\cdot, \cdot)$ to represent the L^2 inner product, and $\langle \cdot, \cdot \rangle$ to denote the duality between a space and its dual. To avoid ambiguity, we use the same notation $\langle \cdot, \cdot \rangle$ for different dualities, and it can occasionally be treated as the L^2 inner product for certain functions. We use the subscript "$\cdot_h$" to denote the dependence on triangulation. In particular, an operator with the subscript "$\cdot_h$" indicates that the operation is performed cell by cell. In addition, $\|\cdot\|_{1,h}$ denotes the piecewise $\boldsymbol{H}^1$-norm $\|\boldsymbol{v}\|_{1,h}^2 = \sum_{T \in \mathcal{T}_h} \|\boldsymbol{v}\|_{1,T}^2$. Finally, $\eqsim$ denotes equality up to a constant. The hidden constants depend on the domain, and when triangulation is involved, they also depend on the shape regularity of the triangulation, but not on h or any other mesh parameter.

The two complexes below are well known:

$$\{0\} \xrightarrow{\text{inc}} H_0^1(\Omega) \xrightarrow{\text{curl}} \boldsymbol{H}_0(\text{div}, \Omega) \xrightarrow{\text{div}} L_0^2(\Omega) \xrightarrow{\int_\Omega \cdot} \{0\}, \tag{1.1}$$

$$\{0\} \xrightarrow{\text{inc}} H_0^2(\Omega) \xrightarrow{\text{curl}} \boldsymbol{H}_0^1(\Omega) \xrightarrow{\text{div}} L_0^2(\Omega) \xrightarrow{\int_\Omega \cdot} \{0\}. \tag{1.2}$$

We refer to [1, 2] for related discussion on more complexes and finite elements.

The fundamental incompressible Stokes problem is

$$\begin{cases} -\varepsilon^2 \Delta \boldsymbol{u} + \nabla p = \boldsymbol{f}, & \text{in } \Omega, \\ \text{div}\, \boldsymbol{u} = 0, & \text{in } \Omega, \\ \boldsymbol{u} = 0, & \text{on } \partial\Omega. \end{cases} \tag{1.3}$$

Here, $\boldsymbol{u}$ is the velocity field, p is the pressure field of the incompressible flow, and ε^2 is the inverse of the Reynolds number, which can be small. The equation's variational formulation is to find $(\boldsymbol{u}, p) \in \boldsymbol{H}_0^1(\Omega) \times L_0^2(\Omega)$ such that

$$\begin{cases} \varepsilon^2\big(\nabla \boldsymbol{u}, \nabla \boldsymbol{v}\big) - (\text{div}\, \boldsymbol{v}, p) & = (\boldsymbol{f}, \boldsymbol{v}), \quad \forall\, \boldsymbol{v} \in \boldsymbol{H}_0^1(\Omega), \\ (\text{div}\, \boldsymbol{u}, q) & = 0, \qquad\quad \forall\, q \in L_0^2(\Omega). \end{cases} \tag{1.4}$$

2 Preliminaries

2.1 Triangulations

Let $\mathcal{T}_h$ be a shape-regular triangular subdivision of Ω with the mesh size h such that $\overline{\Omega} = \cup_{T\in\mathcal{T}_h}\overline{T}$. Denote $\mathcal{X}_h, \mathcal{X}_h^i, \mathcal{X}_h^b, \mathcal{E}_h, \mathcal{E}_h^i, \mathcal{E}_h^b, \mathcal{T}_h$, and $\mathcal{T}_h^i$ as the set of vertices, interior vertices, boundary vertices, edges, interior edges, boundary edges, cells, and cells with three interior edges, respectively. For any edge $e \in \mathcal{E}_h$, denote $\mathbf{n}_e$ and $\mathbf{t}_e$ as the globally defined unit normal and tangential vectors of e, respectively. The subscript $\cdot_e$ can be dropped when there is no ambiguity.

Denote (see Fig. 1a)

$$\mathcal{X}_h^{b,+1} := \{a \in \mathcal{X}_h^i,\ a \text{ is connected to } \mathcal{X}_h^b \text{ by } e \in \mathcal{E}_h^i\}, \text{ and } \mathcal{X}_h^{i,-1} := \mathcal{X}_h^i \setminus \mathcal{X}_h^{b,+1};$$

further, denote with $\mathcal{X}_h^{i,-(k-1)} \neq \emptyset$,

$$\mathcal{X}_h^{b,+k} := \{a \in \mathcal{X}_h^{i,-(k-1)},\ a \text{ is connected to } \mathcal{X}_h^{b,+(k-1)} \text{ by } e \in \mathcal{E}_h^i\}$$

and

$$\mathcal{X}_h^{i,-k} := \mathcal{X}_h^{i,-(k-1)} \setminus \mathcal{X}_h^{b,+k}.$$

The smallest k such that $\mathcal{X}_h^{i,-(k-1)} = \mathcal{X}_h^{b,+k}$ is called the number of layers of the triangulation.

We call $\mathcal{X}_h^{b,+k}$ the k-layer boundary vertices and particularly $\mathcal{X}_h^b := \mathcal{X}_h^{b,+0}$ the 0-layer boundary vertices. Consequently, the $\mathcal{X}_h^{i,-k} = \mathcal{X}_h \backslash \underset{s=0:k}{\cup} \mathcal{X}_h^{b,+s}$ is a collection of all vertices except vertices from the 0-layer to k-layer.

On the triangle T with vertices $\{a_1, a_2, a_3\}$ and edges $\{e_1, e_2, e_3\}$, we denote local unit outward normal vectors by $\{\mathbf{n}_{T,e_1}, \mathbf{n}_{T,e_2}, \mathbf{n}_{T,e_3}\}$ and local unit tangential vectors $\{\mathbf{t}_{T,e_1}, \mathbf{t}_{T,e_2}, \mathbf{t}_{T,e_3}\}$ such that $\mathbf{n}_{T,e_i} \times \mathbf{t}_{T,e_i} > 0$, $i \in \{1, 2, 3\}$; see Fig. 1(b) for an illustration.

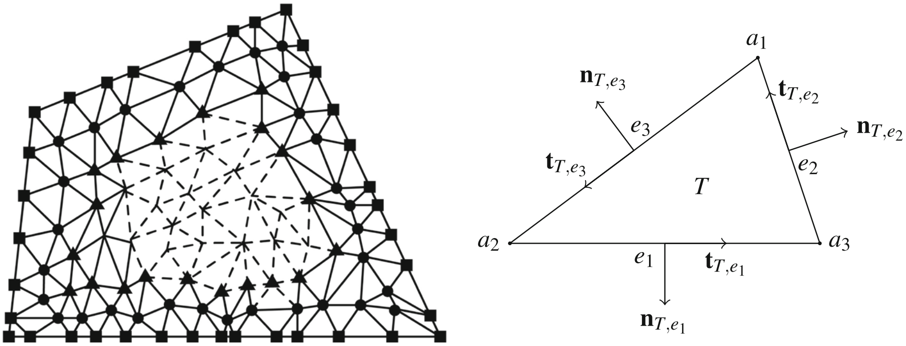

(a) vertex layers: the ■'s denote boundary vertices, the •'s denote vertices of $\mathscr{X}_h^{b,+1}$, and the ▲'s denote vertices of $\mathscr{X}_h^{b,+2}$.

(b) a reference triangle

Fig. 1 A grid with vertices labeled differently, as positions, and a reference cell

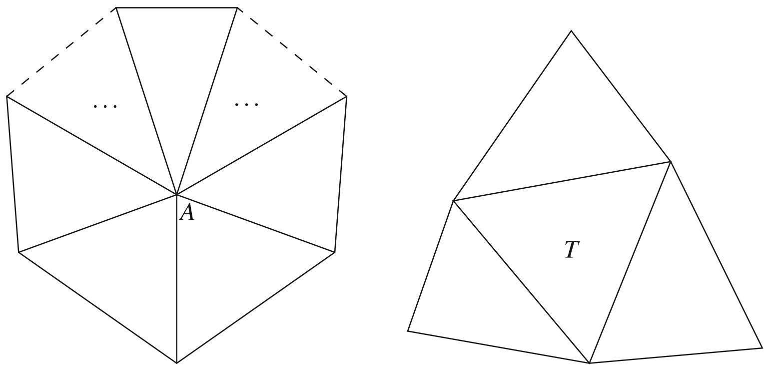

(a) interior vertex patch P_A

(b) interior cell patch P_T

Fig. 2 Illustration of the supports of two types of patches

In addition $\{\lambda_1, \lambda_2, \lambda_3\}$ are the barycentric coordinates with respect to the three corners of T. Also, we denote the lengths of edges by $\{d_1, d_2, d_3\}$, the area of T is S_T, and we drop the subscript when no ambiguity exists. Particularly, $\tilde{S}_{\triangle(A_i,A_j,A_k)}$ represents the directed area of an triangle of corners A_i, A_j, and A_k sequentially, that is, $\tilde{S}_{\triangle(A_i,A_j,A_k)} = \overrightarrow{A_iA_j} \times \overrightarrow{A_iA_k}$.

Next, we figure out two types of patches: combinations of cells.

Interior vertex patch: For the interior vertex A, the cells that connect to A form a (closed) interior vertex patch, denoted by P_A (see Fig. 2a);

Interior cell patch: For the interior cell T, three neighbored cells and T form an interior cell patch, denoted by P_T (see Fig. 2b).

The number of interior vertex patches is $\#\mathscr{X}_h^i$, and the number of interior cell patches is $\#\mathscr{T}_h^i (= 2\#\mathscr{X}_h^i - 2)$.

In the sequel, we make a mild assumption about the grid.

Assumption 2.1 Every boundary vertex is connected to at least one interior vertex.

This assumption assures that every cell is covered by at least one interior vertex patch.

2.2 Polynomial Spaces on a Triangle

For the triangle T, we use $P_k(T)$ to denote the set of polynomials on the T of degrees not higher than k. In a similar manner, $P_k(e)$ is defined on the edge e. We define $\boldsymbol{P}_k(T) = (P_k(T))^2$, and similarly, $\boldsymbol{P}_k(e)$ is defined.

Following [25], we introduce the shape function space as

$$\boldsymbol{P}^{\mathrm{MTW}}(T) := \{\boldsymbol{v} \in \boldsymbol{P}_3(T) : \boldsymbol{v}\cdot\mathbf{n}|_{e_i} \in P_1(e_i),\ i = 1:3,\ \operatorname{div}\boldsymbol{v} \text{ is a constant on } T\}.$$

It can be verified (cf. [14]) that

$$\boldsymbol{P}^{\mathrm{MTW}}(T) = \boldsymbol{P}_1(T) \oplus \operatorname{span}\{\operatorname{curl}(\lambda_i^2\lambda_j\lambda_k)\}_{\{i,j,k\}=\{1,2,3\}}.$$

Following [14], we introduce the shape functions space as

$$\boldsymbol{P}^{\mathrm{GN}-1}(T) = \boldsymbol{P}_1(T) \oplus \operatorname{span}\{\operatorname{curl}(\lambda_i^2\lambda_j^2\lambda_k)\}_{\{i,j,k\}=\{1,2,3\}}.$$

We further denote that

$$\begin{aligned}\boldsymbol{P}^{2-}(T) :&= \boldsymbol{P}_1(T) \oplus \operatorname{span}\{\lambda_i\lambda_j\mathbf{t}_k\}_{\{i,j,k\}=\{1,2,3\}}, \quad \text{and}\\ \boldsymbol{P}^{1+}(T) :&= \boldsymbol{P}_1(T) \oplus \operatorname{span}\{\operatorname{curl}(\lambda_1\lambda_2\lambda_3)\}.\end{aligned}$$

It can be verified that $\boldsymbol{P}^{1+}(T) \subset \boldsymbol{P}^{2-}(T)$,

$$\boldsymbol{P}^{2-}(T) = \{\boldsymbol{v} \in \boldsymbol{P}_2(T) : \boldsymbol{v}\cdot\mathbf{n}|_{e_i} \in P_1(e_i),\ i = 1:3\},$$

and

$$\boldsymbol{P}^{1+}(T) = \{\boldsymbol{v} \in \boldsymbol{P}^{2-}(T) : \operatorname{div}\boldsymbol{v} \text{ is a constant on } T\}.$$

Further we denote that

$$P^{2+}(T) := P_2(T) \oplus \operatorname{span}\{\lambda_1\lambda_2\lambda_3\}.$$

Lemma 2.1 *The two exact sequences hold:*

$$\mathbb{R} \xrightarrow{\text{inc}} P^{2+}(T) \xrightarrow{\text{curl}} \boldsymbol{P}^{2-}(T) \xrightarrow{\text{div}} P_1(T), \tag{2.1}$$

and

$$\mathbb{R} \xrightarrow{\text{inc}} P^{2+}(T) \xrightarrow{\text{curl}} \boldsymbol{P}^{1+}(T) \xrightarrow{\text{div}} P_0(T). \tag{2.2}$$

Proof Noting that $\boldsymbol{P}^{2-}(T)$ is exactly the local shape functions space of the quadratic BDFM element, $\operatorname{div}\boldsymbol{P}^{2-}(T) = P_1(T)$ is well known. Evidently, $\operatorname{curl} P^{2+}(T) \subset \{\boldsymbol{v} \in \boldsymbol{P}^{2-}(T) : \operatorname{div}\boldsymbol{v} = 0\}$ and $\dim(\operatorname{curl} P^{2+}(T)) = \dim(P^{2+}(T)) - 1 = \dim(\boldsymbol{P}^{2-}(T)) - \dim(P_1(T)) = \dim(\{\boldsymbol{v} \in \boldsymbol{P}^{2-}(T) : \operatorname{div}\boldsymbol{v} = 0\})$, thus $\operatorname{curl} P^{2+}(T) = \{\boldsymbol{v} \in \boldsymbol{P}^{2-}(T) : \operatorname{div}\boldsymbol{v} = 0\}$. The proof of (2.1) is completed. Similarly, $\operatorname{div}\boldsymbol{P}^{1+}(T) = P_0(T)$ follows the definition of $\boldsymbol{P}^{1+}(T)$, and (2.2) can be proved the same way. □

Next, we introduce some functions on a cell, and we call them atom basis functions. Defined for $i = 1:3$, $\boldsymbol{w}_{T,e_i} := \operatorname{curl}(\lambda_j\lambda_k(3\lambda_i - 1))$, $\boldsymbol{w}_{T,e_j,e_k} := \operatorname{curl}(\lambda_i^2)$ and $\boldsymbol{\eta}_{T,e_j,e_k} := -\frac{2}{d_i}\lambda_i\mathbf{n}_{T,e_i}$. It holds immediately that $\operatorname{div}\boldsymbol{w}_{T,e_i} = 0$, $\operatorname{div}\boldsymbol{w}_{T,e_j,e_k} = 0$ and $\operatorname{div}\boldsymbol{\eta}_{T,e_j,e_k} = \frac{1}{S}$. This also indicates that $\boldsymbol{w}_{T,e_i}$ is a function with vanishing normal components and tangential integral on the edges e_j and e_k, and $\boldsymbol{w}_{T,e_j,e_k}$ on the edge e_i is similar. For instance, refer to Fig. 3 for an illustration of supports of $\boldsymbol{w}_{T,e_1}$, $\boldsymbol{w}_{T,e_2,e_3}$ and $\boldsymbol{\eta}_{T,e_2,e_3}$.

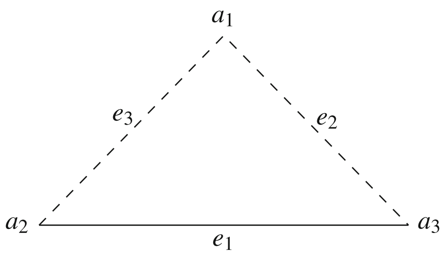

(a) $\boldsymbol{w}_{T,e_1}$ **(b)** $\boldsymbol{w}_{T,e_2,e_3}$ or $\boldsymbol{\eta}_{T,e_2,e_3}$

Fig. 3 Illustration of the supports of atom basis functions; degrees of freedom vanish on dotted edges

Then,

$$\boldsymbol{Z}_T := \{\boldsymbol{v} \in \boldsymbol{P}^{2-}(T) : \operatorname{div} \boldsymbol{v} = 0\} = \{\boldsymbol{v} \in \boldsymbol{P}^{1+}(T) : \operatorname{div} \boldsymbol{v} = 0\}$$
$$= \operatorname{span}\{\boldsymbol{w}_{T,e_1}, \boldsymbol{w}_{T,e_2}, \boldsymbol{w}_{T,e_3}, \boldsymbol{w}_{T,e_2,e_3}, \boldsymbol{w}_{T,e_3,e_1}, \boldsymbol{w}_{T,e_1,e_2}\}$$

and

$$\boldsymbol{P}^{1+}(T) = \operatorname{span}\{\boldsymbol{w}_{T,e_1}, \boldsymbol{w}_{T,e_2}, \boldsymbol{w}_{T,e_3}, \boldsymbol{w}_{T,e_2,e_3}, \boldsymbol{w}_{T,e_3,e_1}, \boldsymbol{w}_{T,e_1,e_2}, \boldsymbol{\eta}_{T,e_2,e_3}, \boldsymbol{\eta}_{T,e_3,e_1}, \boldsymbol{\eta}_{T,e_1,e_2}\}. \tag{2.3}$$

Indeed, the functions of the set in (2.3) are not linearly independent. Any one among $\{\boldsymbol{\eta}_{T,e_2,e_3}, \boldsymbol{\eta}_{T,e_3,e_1}, \boldsymbol{\eta}_{T,e_1,e_2}\}$ together with $\{\boldsymbol{w}_{T,e_1}, \boldsymbol{w}_{T,e_2}, \boldsymbol{w}_{T,e_3}, \boldsymbol{w}_{T,e_2,e_3}, \boldsymbol{w}_{T,e_3,e_1}, \boldsymbol{w}_{T,e_1,e_2}\}$ forms a set of independent bases of $\boldsymbol{P}^{1+}(T)$.

2.3 Some Known Finite Elements

The Madal–Tai–Winther element (see [25]) is defined as

(1) T is a triangle;
(2) $P_T = \boldsymbol{P}^{MTW}(T)$;
(3) for any $\boldsymbol{v} \in (H^1(T))^2$, the nodal functionals on T, denoted by D_T, are $\{\fint_{e_i} \boldsymbol{v} \cdot \mathbf{n}_{T,e_i} d\tau, \fint_{e_i} \boldsymbol{v} \cdot \mathbf{n}_{T,e_i}(\lambda_j - \lambda_k) d\tau, \fint_{e_i} \boldsymbol{v} \cdot \mathbf{t}_{T,e_i} d\tau\}_{i=1:3}$.

Following [25], we introduce

$$\boldsymbol{V}_h^{\mathrm{MTW}} = \{\boldsymbol{v}_h \in \boldsymbol{H}(\operatorname{div}, \Omega) : \boldsymbol{v}_h|_T \in \boldsymbol{P}^{\mathrm{MTW}}(T), \int_e \boldsymbol{v} \cdot \mathbf{t} \text{ is continuous across interior edge } e\},$$

and

$$\boldsymbol{V}_{h0}^{\mathrm{MTW}} := \{\boldsymbol{v}_h \in \boldsymbol{V}_h^{\mathrm{MTW}} \cap \boldsymbol{H}_0(\operatorname{div}, \Omega) : \int_e \boldsymbol{v} \cdot \mathbf{t} = 0 \text{ on boundary edge } e\}.$$

The lowest-degree Guzman–Neilan element (see [14]) is defined as

(1) T is a triangle;
(2) $P_T = \boldsymbol{P}^{\mathrm{GN-1}}(T)$;
(3) for any $\boldsymbol{v} \in (H^1(T))^2$, the nodal functionals on T, denoted by D_T, are $\{\fint_{e_i} \boldsymbol{v} \cdot \mathbf{n}_{T,e_i} d\tau, \fint_{e_i} \boldsymbol{v} \cdot \mathbf{n}_{T,e_i}(\lambda_j - \lambda_k) d\tau, \fint_{e_i} \boldsymbol{v} \cdot \mathbf{t}_{T,e_i} d\tau\}_{i=1:3}$.

Following [14], we introduce

$$\boldsymbol{V}_h^{\mathrm{GN}-1} := \{\boldsymbol{v}_h \in \boldsymbol{H}(\mathrm{div}, \Omega) : \boldsymbol{v}_h|_T \in P^{\mathrm{GN}-1}(T),\ \int_e \boldsymbol{v}\cdot\mathbf{t} \text{ is continuous across interior edge } e\},$$

and

$$\boldsymbol{V}_{h0}^{\mathrm{GN}-1} := \{\boldsymbol{v}_h \in \boldsymbol{V}_h^{\mathrm{GN}-1} \cap \boldsymbol{H}_0(\mathrm{div}, \Omega) : \int_e \boldsymbol{v}\cdot\mathbf{t} = 0 \text{ on boundary edge } e\}.$$

Following Zeng-Zhang-Zhang [37], introduce

$$\boldsymbol{V}_h^{\mathrm{ZZZ}} := \{\boldsymbol{v}_h \in \boldsymbol{H}(\mathrm{div}, \Omega) : \boldsymbol{v}_h|_T \in \boldsymbol{P}_2(T),\ \int_e \boldsymbol{v}\cdot\mathbf{t} \text{ is continuous across interior edge } e\},$$

and

$$\boldsymbol{V}_{h0}^{\mathrm{ZZZ}} := \{\boldsymbol{v}_h \in \boldsymbol{V}_h^{\mathrm{ZZZ}} \cap \boldsymbol{H}_0(\mathrm{div}, \Omega) : \int_e \boldsymbol{v}\cdot\mathbf{t} = 0 \text{ on boundary edge } e\}.$$

As revealed by [37], the space can be viewed as a reduced second-order Brezzi–Douglas–Marini element space with enhanced smoothness.

2.4 Stenberg's Macroelement Technique for the Inf-sup Condition (cf. [31])

A macro-element partition of $\mathscr{T}_h$, denoted by $\mathscr{M}_h$, is a set of macroelements satisfying that each triangle of $\mathscr{T}_h$ is covered by at least one macroelement in $\mathscr{M}_h$.

Definition 2.1 Two macroelements M_1 and M_2 are said to be equivalent if there exists a continuous one-to-one mapping $G : M_1 \to M_2$, such that

(a) $G(M_1) = M_2$;
(b) if $M_1 = \bigcup_{i=1:m}^{m} T_i^1$, then $T_i^2 = G(T_i^1)$ with $i = 1 : m$ are the cells of M_2;
(c) $G|_{T_i^1} = F_{T_i^2} \circ F_{T_i^1}^{-1}$, $i = 1 : m$, where $F_{T_i^1}$ and $F_{T_i^2}$ are the mappings from a reference element $\hat{T}$ onto T_i^1 and T_i^2, respectively.

In addition, a class of equivalent macroelements is a set in which any two macroelements are equivalent to each other.

Next, we introduce some spaces defined on the macroelement M locally. As a subspace of $\boldsymbol{V}_h$, $\boldsymbol{V}_{h0,M}$ consists of functions in $\boldsymbol{V}_h$ that are equal to zero outside M; for any $\boldsymbol{v}_h \in \boldsymbol{V}_{h0,M}$, continuity constraints of $\boldsymbol{V}_h$ enable its corresponding nodal functionals on ∂M to be zero. Similarly, $Q_{h,M}$ is a subspace of Q_h, and it consists of functions that are equal to zero outside M. Denote

$$N_M := \{q_h \in Q_{h,M} : \int_M \mathrm{div}\, \boldsymbol{v}_h\, q_h\, dM = 0, \forall\, \boldsymbol{v}_h \in \boldsymbol{V}_{h0,M}\}. \tag{2.4}$$

Stenberg's macroelement technique can be summarized as the following proposition:

Proposition 2.1 *Suppose there exists the macroelement partitioning $\mathscr{M}_h$ with the fixed set of equivalence classes $\mathbb{E}_i$ of macroelements, $i = 1, 2, ..., n$, a positive integer N (n and N are independent of h), and an operator $\Pi : \boldsymbol{H}_0^1(\Omega) \to \boldsymbol{V}_{h0}$ such that*

(C_1) for each $M \in \mathbb{E}_i$, $i = 1, 2, ..., n$, the space N_M defined in (2.4) is one-dimensional, which consists of functions that are constant on M;
(C_2) each $M \in \mathscr{M}_h$ belongs to one of the classes $\mathbb{E}_i$, $i = 1, 2, ..., n$;

(C_3) each $e \in \mathscr{E}_h^i$ is an interior edge of at least one and no more than N macroelements;
(C_4) for any $\boldsymbol{w} \in \boldsymbol{H}_0^1(\Omega)$, it holds that

$$\sum_{T \in \mathscr{T}_h} h_T^{-2} \|\boldsymbol{w} - \Pi \boldsymbol{w}\|_{0,T}^2 + \sum_{e \in \mathscr{E}_h^i} h_e^{-1} \|\boldsymbol{w} - \Pi \boldsymbol{w}\|_{0,e}^2 \leq C \|\boldsymbol{w}\|_{1,\Omega}^2 \quad \text{and} \quad \|\Pi \boldsymbol{w}\|_{1,h} \leq C \|\boldsymbol{w}\|_{1,\Omega}.$$

Then, the uniform inf-sup condition holds for the finite element pair.

3 An Auxiliary Stable Pair for the Stokes Problem

3.1 An sBDFM Element

We define the sBDFM element by

(1) T is a triangle;
(2) $P_T = \boldsymbol{P}^{2-}(T)$;
(3) for any $\boldsymbol{v} \in (H^1(T))^2$, the nodal functionals on T, denoted by D_T, are $\{⨍_{e_i} \boldsymbol{v} \cdot \mathbf{n}_{T,e_i} d\tau,\ ⨍_{e_i} \boldsymbol{v} \cdot \mathbf{n}_{T,e_i} (\lambda_j - \lambda_k) d\tau,\ ⨍_{e_i} \boldsymbol{v} \cdot \mathbf{t}_{T,e_i} d\tau\}_{i=1:3}$.

The above triple is P_T−unisolvent. We use $\boldsymbol{\varphi}_{\mathbf{n}_{T,e_i},0}$, $\boldsymbol{\varphi}_{\mathbf{n}_{T,e_i},1}$, and $\boldsymbol{\varphi}_{\mathbf{t}_{T,e_i},0}$ to represent the corresponding nodal basis functions, and then

$$\begin{cases} \boldsymbol{\varphi}_{\mathbf{n}_{T,e_i},0} = \lambda_j(3\lambda_j - 2)\dfrac{\mathbf{t}_{T,e_k}}{(\mathbf{n}_{T,e_i}, \mathbf{t}_{T,e_k})} + \lambda_k(3\lambda_k - 2)\dfrac{\mathbf{t}_{T,e_j}}{(\mathbf{n}_{T,e_i}, \mathbf{t}_{T,e_j})} + 6\lambda_j\lambda_k \mathbf{n}_{T,e_i}; \\ \boldsymbol{\varphi}_{\mathbf{n}_{T,e_i},1} = 3\lambda_j(3\lambda_j - 2)\dfrac{\mathbf{t}_{T,e_k}}{(\mathbf{n}_{T,e_i}, \mathbf{t}_{T,e_k})} - 3\lambda_k(3\lambda_k - 2)\dfrac{\mathbf{t}_{T,e_j}}{(\mathbf{n}_{T,e_i}, \mathbf{t}_{T,e_j})}; \\ \boldsymbol{\varphi}_{\mathbf{t}_{T,e_i},0} = 6\lambda_j\lambda_k \mathbf{t}_{T,e_i}. \end{cases} \tag{3.1}$$

We use $\boldsymbol{V}_h^{\mathrm{sBDFM}}$ and $\boldsymbol{V}_{h0}^{\mathrm{sBDFM}}$ for the corresponding finite element spaces, where the subscript $\cdot_{h0}$ implies that the nodal functionals along the boundary of the domain are all zero.

$$\begin{aligned} \boldsymbol{V}_h^{\mathrm{sBDFM}} := \Big\{ & \boldsymbol{v}_h \in \boldsymbol{L}^2(\Omega) : \boldsymbol{v}_h|_T \in \boldsymbol{P}^{2-}(T), \forall T \in \mathscr{T}_h; \\ & ⨍_e (\boldsymbol{v} \cdot \mathbf{n}_e)\tau^s d\tau (s = 0, 1) \text{ and } ⨍_e \boldsymbol{v} \cdot \mathbf{t}_e d\tau \text{ are continuous}, \forall e \in \mathscr{E}_h^i \Big\}. \end{aligned} \tag{3.2}$$

$$\boldsymbol{V}_{h0}^{\mathrm{sBDFM}} := \left\{ \boldsymbol{v}_h \in \boldsymbol{V}_h^{\mathrm{sBDFM}} : ⨍_e (\boldsymbol{v} \cdot \mathbf{n}_e)\tau^s d\tau = 0 (s = 0, 1) \text{ and } ⨍_e \boldsymbol{v} \cdot \mathbf{t}_e d\tau \text{ vanish}, \forall e \in \mathscr{E}_h^b \right\}. \tag{3.3}$$

Evidently, it holds that

$$\boldsymbol{\varphi} \cdot \mathbf{n}_{T,e_j}|_{e_j} \in P_1(e_j),\ j = 1:3,\ \forall \boldsymbol{\varphi} \in \{\boldsymbol{\varphi}_{\mathbf{n}_{T,e_i},0}, \boldsymbol{\varphi}_{\mathbf{n}_{T,e_i},1}, \boldsymbol{\varphi}_{\mathbf{t}_{T,e_i},0}\},\ i = 1:3.$$

Therefore, $\boldsymbol{V}_h^{\mathrm{sBDFM}}$ is a smoothened subspace of the famous second-order BDFM element space. Indeed, $\boldsymbol{V}_h^{\mathrm{sBDFM}} \subset \boldsymbol{H}(div, \Omega)$ but $\boldsymbol{V}_h^{\mathrm{sBDFM}} \not\subset \boldsymbol{H}^1(\Omega)$, and $\boldsymbol{V}_{h0}^{\mathrm{sBDFM}}$ is similar.

We define a nodal interpolation operator $\Pi_h : \boldsymbol{H}^1(\Omega) \to \boldsymbol{V}_h^{\mathrm{sBDFM}}$ such that for any $e \subset \mathscr{E}_h$,

$$⨍_e (\Pi_h \boldsymbol{v} \cdot \mathbf{n}_e) p = ⨍_e (\boldsymbol{v} \cdot \mathbf{n}_e) p,\ \forall p \in P_1(e) \quad \text{and} \quad ⨍_e \Pi_h \boldsymbol{v} \cdot \mathbf{t}_e = ⨍_e \boldsymbol{v} \cdot \mathbf{t}_e.$$

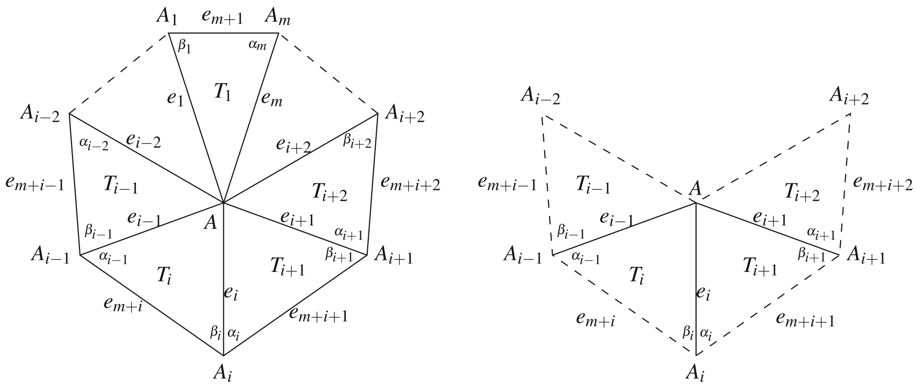

Fig. 4 Illustration of the patch around A and its part amplification

The operator Π_h is locally defined on each triangle, and it preserves linear functions locally. Furthermore, the local space $\boldsymbol{P}^{2-}(T)$ is invariant under the Piola's transformation; that is, it maps $\boldsymbol{P}^{2-}(T)$ onto $\boldsymbol{P}^{2-}(\hat{T})$. Therefore, approximation estimates of Π_h can be derived from Lemma 2.1.5 and Remark 2.1.8 in [6], along with standard scaling arguments and the Bramble–Hilbert lemma.

Proposition 3.1 *It holds for* $k \le s$, $1 < s \le 2$ *that*

$$|\boldsymbol{v} - \Pi_h \boldsymbol{v}|_{k,h} \le C h^{s-k} |\boldsymbol{v}|_{s,\Omega}, \quad \forall\, \boldsymbol{v} \in \boldsymbol{H}^s(\Omega).$$

3.2 Structure of the Kernel of div on a Closed Patch

For the $m-$cell interior vertex patch P_A, we label cells of it sequentially as $T_i, i = 1 : m$, and label $e_i = \overline{T_i} \cap \overline{T_{i+1}}$ $(i = 1 : m - 1)$, $e_m = \overline{T_m} \cap \overline{T_1}$. Also, we label e_{m+i} $(i = 1 : m)$ as the edge opposite to A in T_i; we refer to Fig. 4a for an illustration.

Viewing P_A as a special grid, we can construct $\boldsymbol{V}_{h0}^{\mathrm{sBDFM}}(P_A)$ as follows:

$$\boldsymbol{V}_{h0}^{\mathrm{sBDFM}}(P_A) := \Big\{ \boldsymbol{v}_h \in \boldsymbol{L}^2(P_A) : \boldsymbol{v}_h|_T \in \boldsymbol{P}^{2-}(T_i),\ i = 1 : m;$$
$$\fint_e (\boldsymbol{v} \cdot \mathbf{n}_e)\tau^s d\tau\,(s = 0, 1) \text{ and } \fint_e (\boldsymbol{v} \cdot \mathbf{t}_e) d\tau \text{ are continuous across } e = e_i,\ i = 1 : m,$$
$$\text{and vanish on } e = e_j,\ j = m + 1 : 2m \Big\}. \tag{3.4}$$

Denote

$$\boldsymbol{Z}_A := \{\boldsymbol{v} \in \boldsymbol{V}_{h0}^{\mathrm{sBDFM}}(P_A) : \operatorname{div} \boldsymbol{v} = 0\}.$$

Lemma 3.1 $\dim(\boldsymbol{Z}_A) = 1$.

Proof Assume $\boldsymbol{\psi}_h \in \boldsymbol{Z}_A$, then $\boldsymbol{\psi}_h|_{T_i} \subset \boldsymbol{Z}_{T_i}$, $i = 1 : m$. By the boundary conditions, it follows that

$$\begin{cases} \boldsymbol{\psi}_h|_{T_1} = \gamma_{T_1}^m \boldsymbol{w}_{T_1,e_m} + \gamma_{T_1}^1 \boldsymbol{w}_{T_1,e_1} + \gamma_{T_1}^{m,1} \boldsymbol{w}_{T_1,e_m,e_1}, \\ \boldsymbol{\psi}_h|_{T_i} = \gamma_{T_i}^{i-1} \boldsymbol{w}_{T_i,e_{i-1}} + \gamma_{T_i}^{i} \boldsymbol{w}_{T_i,e_i} + \gamma_{T_i}^{i-1,i} \boldsymbol{w}_{T_i,e_{i-1},e_i}, \ (i = 2 : m-1) \\ \boldsymbol{\psi}_h|_{T_m} = \gamma_{T_m}^{m-1} \boldsymbol{w}_{T_m,e_{m-1}} + \gamma_{T_m}^{m} \boldsymbol{w}_{T_m,e_m} + \gamma_{T_m}^{m-1,m} \boldsymbol{w}_{T_m,e_{m-1},e_m}, \end{cases} \tag{3.5}$$

with $\gamma_{T_1}^m$, $\gamma_{T_1}^1$, $\gamma_{T_1}^{m,1}$, $\gamma_{T_m}^{m-1}$, $\gamma_{T_m}^m$, $\gamma_{T_m}^{m-1,m}$ and $\gamma_{T_i}^{i-1}$, $\gamma_{T_i}^i$, $\gamma_{T_i}^{i-1,i}$ $(i = 2 : m-1)$ determined such that $\boldsymbol{\psi}_h$ satisfies the continuity restriction of $\boldsymbol{V}_h^{\mathrm{sBDFM}}$.

For an arbitrary edge e_i, $1 \le i \le m$, across it, the normal component of $\boldsymbol{\psi}_h$ and integration of the tangential component of $\boldsymbol{\psi}_h$ are continuous; see Fig. 4b for an illustration. Based on the continuity conditions, a direct calculation shows that

$$\gamma_{T_i}^{i-1,i} = \gamma_{T_{i+1}}^{i,i+1}$$

and

$$\begin{cases} \gamma_{T_i}^i = \dfrac{\tilde{S}_{\triangle(A_i,A_{i+1},A_{i-1})}}{S_i + S_{i+1}} \gamma_{T_i}^{i-1,i}, \\ \gamma_{T_{i+1}}^i = \dfrac{\tilde{S}_{\triangle(A_i,A_{i+1},A_{i-1})}}{S_i + S_{i+1}} \gamma_{T_{i+1}}^{i,i+1}. \end{cases} \tag{3.6}$$

By checking weak tangential continuity conditions of $\boldsymbol{V}_h^{\mathrm{sBDFM}}$ on all edges e_i, $i = 1 : m$, we have

$$\gamma_{T_1}^{m,1} = \gamma_{T_2}^{1,2} = \ldots = \gamma_{T_m}^{m-1,m}. \tag{3.7}$$

Now, we choose $\gamma_{T_1}^{m,1} = 1$ in (3.7) and it follows that

$$\gamma_{T_1}^{m,1} = \gamma_{T_2}^{1,2} = \ldots = \gamma_{T_m}^{m-1,m} = 1. \tag{3.8}$$

Substituting (3.8) into the counterparts of (3.6) on every cell T_i, $i = 1 : m$, we have

$$\begin{cases} \gamma_{T_1}^m = \dfrac{\tilde{S}_{\triangle(A_m,A_1,A_{m-1})}}{S_m + S_1}, \ \gamma_{T_1}^1 = \dfrac{\tilde{S}_{\triangle(A_1,A_2,A_m)}}{S_1 + S_2}, \\ \gamma_{T_i}^{i-1} = \dfrac{\tilde{S}_{\triangle(A_{i-1},A_i,A_{i-2})}}{S_{i-1} + S_i}, \ \gamma_{T_i}^i = \dfrac{\tilde{S}_{\triangle(A_i,A_{i+1},A_{i-1})}}{S_i + S_{i+1}}, \ (i = 2 : m-2) \\ \gamma_{T_m}^{m-1} = \dfrac{\tilde{S}_{\triangle(A_{m-1},A_m,A_{m-2})}}{S_{m-1} + S_m}, \ \gamma_{T_m}^m = \dfrac{\tilde{S}_{\triangle(A_m,A_1,A_{m-1})}}{S_m + S_1}. \end{cases} \tag{3.9}$$

Then, bringing (3.9) back to (3.5) gives

$$\begin{cases} \boldsymbol{\psi}_h|_{T_1} = \dfrac{\tilde{S}_{\triangle(A_m,A_1,A_{m-1})}}{S_m + S_1} \boldsymbol{w}_{T_1,e_m} + \dfrac{\tilde{S}_{\triangle(A_1,A_2,A_m)}}{S_1 + S_2} \boldsymbol{w}_{T_1,e_1} + \boldsymbol{w}_{T_1,e_m,e_1}, \\ \boldsymbol{\psi}_h|_{T_i} = \dfrac{\tilde{S}_{\triangle(A_{i-1},A_i,A_{i-2})}}{S_{i-1} + S_i} \boldsymbol{w}_{T_i,e_{i-1}} + \dfrac{\tilde{S}_{\triangle(A_i,A_{i+1},A_{i-1})}}{S_i + S_{i+1}} \boldsymbol{w}_{T_i,e_i} + \boldsymbol{w}_{T_i,e_{i-1},e_i}, \ (i = 2 : m-1) \\ \boldsymbol{\psi}_h|_{T_m} = \dfrac{\tilde{S}_{\triangle(A_{m-1},A_m,A_{m-2})}}{S_{m-1} + S_m} \boldsymbol{w}_{T_m,e_{m-1}} + \dfrac{\tilde{S}_{\triangle(A_m,A_{m+1},A_{m-1})}}{S_m + S_1} \boldsymbol{w}_{T_m,e_m} + \boldsymbol{w}_{T_m,e_{m-1},e_m}. \end{cases}$$

Now, it is evident that $\boldsymbol{\psi}_h \in \boldsymbol{Z}_A$ and further $\boldsymbol{Z}_A = \mathrm{span}\{\boldsymbol{\psi}_h\}$. The proof is completed. □

3.3 A Stable Conservative Pair for the Stokes Problem

Denote

$\mathbb{P}^1_h(\mathscr{T}_h) := \{q_h \in L^2(\Omega) : q_h|_T \in P_1(T), \forall\, T \in \mathscr{T}_h\}$ and $\mathbb{P}^1_{h0}(\mathscr{T}_h) := \mathbb{P}^1_h(\mathscr{T}_h) \cap L^2_0(\Omega)$.

Then, $\boldsymbol{V}_{h0}^{\mathrm{sBDFM}} \times \mathbb{P}^1_{h0}$ forms a stable pair for the Stokes problem.

Theorem 3.1 (Stability of $\boldsymbol{V}_{h0}^{\mathrm{sBDFM}}$–$\mathbb{P}^1_{h0}$) *Let $\{\mathscr{T}_h\}$ be a family of triangulations of Ω satisfying Assumption 2.1. Then it holds that*

$$\sup_{\boldsymbol{v}_h \in \boldsymbol{V}_{h0}^{\mathrm{sBDFM}}} \frac{(div\ \boldsymbol{v}_h, q_h)}{\|\boldsymbol{v}_h\|_{1,h}} \geq C\|q_h\|_{0,\Omega}, \forall\, q_h \in \mathbb{P}^1_{h0}(\mathscr{T}_h). \tag{3.10}$$

Proof First, for any interior vertex A and its patch P_A, we can construct $\boldsymbol{V}_{h0}^{\mathrm{sBDFM}}(P_A)$ as (3.4) and $\mathbb{P}^1_{h0}(P_A) = \{q_h \in L^2(P_A) : q_h|_T \in P_1(T), \forall\, T \in P_A\} \cap L^2_0(P_A)$. Obviously, $\mathrm{div}\, \boldsymbol{V}_{h0}^{\mathrm{sBDFM}}(P_A) \subset \mathbb{P}^1_{h0}(P_A)$. Thus, counting the dimension, we obtain $\mathrm{div}\, \boldsymbol{V}_{h0}^{\mathrm{sBDFM}}(P_A) = \mathbb{P}^1_{h0}(P_A)$ by Lemma 3.1. This verifies the condition (C_1) of Proposition 2.1. The other conditions of Proposition 2.1 are direct, and the inf-sup condition (3.10) holds by Proposition 2.1. The proof is completed. □

Now consider the finite element discretization: Find $(\boldsymbol{\varphi}_h, p_h) \in \boldsymbol{V}_{h0}^{\mathrm{sBDFM}} \times \mathbb{P}^1_{h0}$, such that

$$\begin{cases} \varepsilon^2(\nabla_h \boldsymbol{\varphi}_h, \nabla_h \boldsymbol{\psi}_h) - (\mathrm{div}\, \boldsymbol{\psi}_h, p_h) = (\boldsymbol{f}, \boldsymbol{\psi}_h), & \forall\, \boldsymbol{\psi}_h \in \boldsymbol{V}_{h0}^{\mathrm{sBDFM}}, \\ (\mathrm{div}\, \boldsymbol{\varphi}_h, q_h) = 0, & \forall\, q_h \in \mathbb{P}^1_{h0}. \end{cases} \tag{3.11}$$

The well-posedness of (3.11) is immediate.

Lemma 3.2 *Given $\boldsymbol{\varphi} \in \boldsymbol{H}^1_0(\Omega) \cap \boldsymbol{H}^2(\Omega)$ such that $\mathrm{div}\, \boldsymbol{\varphi} = 0$, it holds that*

$$\inf_{\boldsymbol{\psi}_h \in \boldsymbol{V}_{h0}^{\mathrm{sBDFM}},\, \mathrm{div}\, \boldsymbol{\psi}_h = 0} \|\boldsymbol{\varphi} - \boldsymbol{\psi}_h\|_{1,h} \leq Ch\|\boldsymbol{\varphi}\|_{2,\Omega}.$$

Proof Let $(\boldsymbol{\varphi}^*, p^*) \in \boldsymbol{H}^1_0(\Omega) \times L^2_0(\Omega)$ be such that

$$\begin{cases} (\nabla \boldsymbol{\varphi}^*, \nabla \boldsymbol{\psi}) - (\mathrm{div}\, \boldsymbol{\psi}, p^*) = (\mathrm{curl}\,\mathrm{rot}\, \boldsymbol{\varphi}, \boldsymbol{\psi}), & \forall\, \boldsymbol{\psi} \in \boldsymbol{H}^1_0(\Omega), \\ (\mathrm{div}\, \boldsymbol{\varphi}^*, q) = 0, & \forall\, q \in L^2_0(\Omega). \end{cases}$$

Then $\boldsymbol{\varphi}^* = \boldsymbol{\varphi}$ and $p^* = 0$. Now let $(\boldsymbol{\varphi}^*_h, p^*_h) \in \boldsymbol{V}_{h0}^{\mathrm{sBDFM}} \times \mathbb{P}^1_{h0}$ be such that

$$\begin{cases} (\nabla_h \boldsymbol{\varphi}^*_h, \nabla_h \boldsymbol{\psi}_h) - (\mathrm{div}\, \boldsymbol{\psi}_h, p^*_h) = (\mathrm{curl}\,\mathrm{rot}\, \boldsymbol{\varphi}, \boldsymbol{\psi}_h), & \forall\, \boldsymbol{\psi}_h \in \boldsymbol{V}_{h0}^{\mathrm{sBDFM}}, \\ (\mathrm{div}\, \boldsymbol{\varphi}^*_h, q_h) = 0, & \forall\, q_h \in \mathbb{P}^1_{h0}. \end{cases} \tag{3.12}$$

Then the second equation of (3.12) together with $\mathrm{div}\boldsymbol{\varphi}^*_h \in \mathbb{P}^1_{h0}$ gives $\mathrm{div}\, \boldsymbol{\varphi}^*_h = 0$, and further it holds that $\|\boldsymbol{\varphi}^* - \boldsymbol{\varphi}^*_h\|_{1,h} \leq Ch\|\boldsymbol{\varphi}\|_{2,\Omega}$. The proof is completed. □

The convergence estimate robustness in ε can be obtained in a standard way (cf. [7]).

Theorem 3.2 *Let $(\boldsymbol{\varphi}, p)$ and $(\boldsymbol{\varphi}_h, p_h)$ be the solutions of (1.4) and (3.11), respectively. If $(\boldsymbol{\varphi}, p) \in \boldsymbol{H}^2(\Omega) \times H^1(\Omega)$, then*

$$|\boldsymbol{u} - \boldsymbol{u}_h|_{1,h} \leq Ch|\boldsymbol{u}|_{2,\Omega}, \quad and \quad \|p - p_h\|_{0,\Omega} \leq C(h|p|_{1,\Omega} + \varepsilon^2 h|\boldsymbol{u}|_{2,\Omega}).$$

4 A Continuous Nonconforming Finite Element Scheme for the Biharmonic Equation

4.1 A Finite Element Stokes Complex

We define

$$V_h^{2+} := \left\{ v_h \in H^1(\Omega) : v_h|_T \in P^{2+}(T),\ \forall T \in \mathcal{T}_h;\ \int_e \frac{\partial v_h}{\partial \mathbf{n}} \text{ is continuous across interior edge } e \right\},$$

and

$$V_{h0}^{2+} := \left\{ v_h \in V_h^{2+} \cap H_0^1(\Omega) : \int_e \frac{\partial v_h}{\partial \mathbf{n}} = 0 \text{ on boundary edge } e \right\}.$$

Lemma 4.1 *The exact sequence holds as*

$$\{0\} \xrightarrow{\text{inc}} V_{h0}^{2+} \xrightarrow{\text{curl}} \boldsymbol{V}_{h0}^{\text{sBDFM}} \xrightarrow{\text{div}} \mathbb{P}_{h0}^1 \xrightarrow{\int_\Omega \cdot} \{0\}.$$

Proof Regarding Theorem 3.1, we only have to show that

$$\{\boldsymbol{v}_h \in \boldsymbol{V}_{h0}^{\text{sBDFM}} : \text{div}\, \boldsymbol{v}_h = 0\} = \text{curl}\, V_{h0}^{2+}.$$

Denote $V_{h0}^{2+,C} := \{v_h \in H_0^1(\Omega) : v_h|_T \in P^{2+}(T),\ \forall T \in \mathcal{T}_h\}$. Given $\boldsymbol{v}_h \in \boldsymbol{V}_{h0}^{\text{sBDFM}} \subset \boldsymbol{H}_0(\text{div}, \Omega)$ such that $\text{div}\, \boldsymbol{v}_h = 0$, by the local exact sequence Lemma 2.1 and the de Rham complex (1.1), there exists a $w_h \in V_{h0}^{2+,C}$, such that $\text{curl}\, w_h = \boldsymbol{v}_h$. Further, by the tangential continuity restriction on $\boldsymbol{v}_h$, it follows that $w_h \in V_{h0}^{2+}$. The proof is completed. □

4.2 A Low-Degree Scheme for the Biharmonic Equation

We consider the following biharmonic equation: given $g \in H^{-1}(\Omega)$, find $u \in H_0^2(\Omega)$, such that

$$(\nabla^2 u, \nabla^2 v) = \langle g, v\rangle, \quad \forall v \in H_0^2(\Omega). \tag{4.1}$$

A finite element discretization is to find $u_h \in V_{h0}^{2+}$, such that

$$(\nabla_h^2 u_h, \nabla_h^2 v_h) = \langle g, v_h\rangle, \quad \forall v_h \in V_{h0}^{2+}. \tag{4.2}$$

Remark 4.1 Note that $V_{h0}^{2+} \subset H_0^1(\Omega)$. For the right hand side $g \in H^{-1}(\Omega)$, no extra interpolation to H^1 functions is needed.

The lemma below is an immediate consequence of Lemmas 3.2 and 4.1:

Lemma 4.2 *It holds for $w \in H^3(\Omega) \cap H_0^2(\Omega)$ that*

$$\inf_{v_h \in V_{h0}^{2+}} \|w - v_h\|_{2,h} \le Ch\|w\|_{3,\Omega}.$$

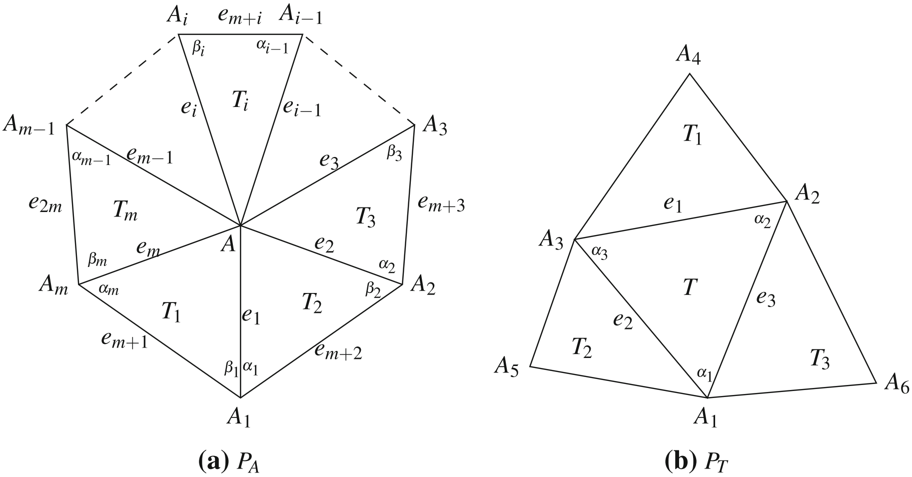

Fig. 5 Illustration of an interior vertex patch and an interior cell patch

Proof By Lemmas 3.2 and 4.1,

$$\begin{aligned}\inf_{v_h\in V_{h0}^{2+}}|w-v_h|_{2,h}&=\inf_{v_h\in V_{h0}^{2+}}|\mathrm{curl}\,w-\mathrm{curl}\,v_h|_{1,h}\\&=\inf_{\boldsymbol{\psi}_h\in \boldsymbol{V}_{h0}^{\mathrm{sBDFM}},\ \mathrm{div}\,\boldsymbol{\psi}_h=0}|\mathrm{curl}\,w-\boldsymbol{\psi}_h|_{1,h}\le Ch|\mathrm{curl}\,w|_{2,\Omega}\le Ch\|w\|_{3,\Omega}.\end{aligned}$$

This completes the proof. □

Theorem 4.1 *Let u and u_h be the solutions of (4.1) and (4.2), respectively, and assume $u\in H^3(\Omega)\cap H_0^2(\Omega)$. Then it holds that*

$$\|u-u_h\|_{2,h}\le Ch\|u\|_{3,\Omega}.$$

The proof of the theorem follows from standard arguments, and we omit it here.

4.3 Basis Functions of V_{h0}^{2+}

For the implementation of the finite element schemes, we present the explicit formulation of the basis functions of certain finite element spaces in this section.

4.3.1 Basis Functions of the Kernel Subspace of the sBDFM Element

Denote the kernel subspace of sBDFM element as

$$\boldsymbol{Z}_{h0}:=\{\boldsymbol{v}_h\in \boldsymbol{V}_{h0}^{\mathrm{sBDFM}}:\mathrm{div}\,\boldsymbol{v}_h=0\}.$$

First, associated with the interior vertex patch around interior vertex A, denote $\boldsymbol{\psi}^A$ as (see Fig. 5a)

$$\boldsymbol{\psi}^A = \begin{cases} \frac{\tilde{S}_{\triangle(A_1,A_2,A_m)}}{S_1+S_2}\boldsymbol{w}_{T_1,e_1} + \frac{\tilde{S}_{\triangle(A_m,A_1,A_{m-1})}}{S_1+S_m}\boldsymbol{w}_{T_1,e_m} + \boldsymbol{w}_{T_1,e_1,e_m}, \ in\ T_1, \\ \frac{\tilde{S}_{\triangle(A_i,A_{i+1},A_{i-1})}}{S_i+S_{i+1}}\boldsymbol{w}_{T_i,e_i} + \frac{\tilde{S}_{\triangle(A_{i-1},A_i,A_{i-2})}}{S_i+S_{i-1}}\boldsymbol{w}_{T_i,e_{i-1}} + \boldsymbol{w}_{T_i,e_i,e_{i-1}}, in\ T_i\ (i=2:m-1), \\ \frac{\tilde{S}_{\triangle(A_m,A_1,A_{m-1})}}{S_m+S_1}\boldsymbol{w}_{T_m,e_m} + \frac{\tilde{S}_{\triangle(A_{m-1},A_m,A_{m-2})}}{S_m+S_{m-1}}\boldsymbol{w}_{T_m,e_{m-1}} + \boldsymbol{w}_{T_m,e_m,e_{m-1}}, \ in\ T_m. \end{cases} \tag{4.3}$$

Second, associated with the interior cell patch around interior cell T, denote $\boldsymbol{\psi}_T$ as (see Fig. 5b)

$$\boldsymbol{\psi}_T = \begin{cases} \frac{S_1}{S_1+S}\boldsymbol{w}_{T_1,e_1}, \ in\ T_1, \\ \frac{S_2}{S_2+S}\boldsymbol{w}_{T_2,e_2}, \ in\ T_2, \\ \frac{S_3}{S_3+S}\boldsymbol{w}_{T_3,e_3}, \ in\ T_3, \\ \frac{1}{3}(\frac{S_1-2S}{S_1+S}\boldsymbol{w}_{T,e_1} + \frac{S_2-2S}{S_2+S}\boldsymbol{w}_{T,e_2} + \frac{S_3-2S}{S_3+S}\boldsymbol{w}_{T,e_3} + \boldsymbol{w}_{T,e_2,e_3} \\ \quad + \boldsymbol{w}_{T,e_3,e_1} + \boldsymbol{w}_{T,e_1,e_2}), \ in\ T. \end{cases} \tag{4.4}$$

Lemma 4.3 *The functions of $\Phi_h(\mathcal{T}_h) := \{\boldsymbol{\psi}^A,\ A \in \mathcal{X}_h^i;\ \boldsymbol{\psi}_T,\ T \in \mathcal{T}_h^i\}$ form a basis of $\boldsymbol{Z}_{h0}$.*

The proof is given in Appendix B.1.

4.3.2 Basis functions of V_{h0}^{2+}

Note that the curl operator is a bijection from V_{h0}^{2+} onto $\boldsymbol{Z}_{h0}$. Therefore, the basis functions of V_{h0}^{2+} are $\{\zeta^A,\ A \in \mathcal{X}_h^i;\ \zeta_T,\ T \in \mathcal{T}_h^i\}$, such that curl $\zeta^A = \boldsymbol{\psi}^A$ and curl $\zeta_T = \boldsymbol{\psi}_T$. More precisely (cf. Fig. 5),

$$\zeta^A = \begin{cases} \lambda^2 + \frac{\tilde{S}_{\triangle(A_1,A_2,A_m)}}{S_1+S_2}\lambda\lambda_1(3\lambda_m-1) + \frac{\tilde{S}_{\triangle(A_m,A_1,A_{m-1})}}{S_1+S_m}\lambda\lambda_m(3\lambda_1-1), \ in\ T_1, \\ \lambda^2 + \frac{\tilde{S}_{\triangle(A_i,A_{i+1},A_{i-1})}}{S_i+S_{i+1}}\lambda\lambda_i(3\lambda_{i-1}-1) + \frac{\tilde{S}_{\triangle(A_{i-1},A_i,A_{i-2})}}{S_i+S_{i-1}}\lambda\lambda_{i-1}(3\lambda_i-1), \ in\ T_i,\ (i=2:m-1) \\ \lambda^2 + \frac{\tilde{S}_{\triangle(A_m,A_1,A_{m-1})}}{S_m+S_1}\lambda\lambda_m(3\lambda_{m-1}-1) + \frac{\tilde{S}_{\triangle(A_{m-1},A_m,A_{m-2})}}{S_m+S_{m-1}}\lambda\lambda_{m-1}(3\lambda_m-1), \ in\ T_m, \end{cases}$$

and

$$\zeta_T = \begin{cases} \frac{S_1}{S_1+S}\lambda_2\lambda_3(3\lambda_4-1), \ in\ T_1, \\ \frac{S_2}{S_1+S}\lambda_1\lambda_3(3\lambda_5-1), \ in\ T_2, \\ \frac{S_3}{S_1+S}\lambda_1\lambda_2(3\lambda_6-1), \ in\ T_3, \\ \frac{S_1}{S_1+S}\lambda_2\lambda_3(3\lambda_1-1) + \frac{S_2}{S_1+S}\lambda_1\lambda_3(3\lambda_2-1) + \frac{S_3}{S_1+S}\lambda_1\lambda_2(3\lambda_3-1) - 6\lambda_1\lambda_2\lambda_3, \ in\ T. \end{cases}$$

5 An Enriched Linear–Constant Finite Element Scheme for Incompressible Flows

5.1 An Enriched Linear Element Space

We define

$$\boldsymbol{V}_h^{\mathrm{el}} := \left\{\boldsymbol{v}_h \in \boldsymbol{H}(\mathrm{div}, \Omega) : \boldsymbol{v}_h|_T \in \boldsymbol{P}^{1+}(T),\ \int_e \boldsymbol{v}_h \cdot \mathbf{t} \text{ is continuous across interior edge } e\right\},$$

and

$$\boldsymbol{V}_{h0}^{\mathrm{el}} := \left\{\boldsymbol{v}_h \in \boldsymbol{V}_h^{\mathrm{el}} \cap \boldsymbol{H}_0(\mathrm{div}, \Omega) : \int_e \boldsymbol{v}_h \cdot \mathbf{t} \text{ vanishes on boundary edge } e\right\}.$$

Remark 5.1 Evidently, $\boldsymbol{V}_h^{\mathrm{el}} = \{\boldsymbol{v}_h \in \boldsymbol{V}_h^{\mathrm{sBDFM}} : \mathrm{div}\, \boldsymbol{v}_h \in \mathbb{P}_{h0}^0\}$, and $\boldsymbol{V}_{h0}^{\mathrm{el}} = \{\boldsymbol{v}_h \in \boldsymbol{V}_{h0}^{\mathrm{sBDFM}} : \mathrm{div}\, \boldsymbol{v}_h \in \mathbb{P}_{h0}^0\}$. Particularly, $\{\boldsymbol{v}_h \in \boldsymbol{V}_{h0}^{\mathrm{el}} : \mathrm{div}\, \boldsymbol{v}_h = 0\} = \{\boldsymbol{v}_h \in \boldsymbol{V}_{h0}^{\mathrm{sBDFM}} : \mathrm{div}\, \boldsymbol{v}_h = 0\}$.

The next lemma is an immediate result of Lemma 4.1 and Remark 5.1:

Lemma 5.1 *The exact sequence holds as*

$$\{0\} \xrightarrow{\mathrm{inc}} V_{h0}^{2+} \xrightarrow{\mathrm{curl}} \boldsymbol{V}_{h0}^{\mathrm{el}} \xrightarrow{\mathrm{div}} \mathbb{P}_{h0}^0 \xrightarrow{\int_\Omega \cdot} \{0\}.$$

Lemma 5.2 $\boldsymbol{V}_{h0}^{\mathrm{el}} = \boldsymbol{V}_{h0}^{\mathrm{ZZZ}} \cap \boldsymbol{V}_{h0}^{\mathrm{MTW}}$.

Proof On on hand, by definition, it holds that $\boldsymbol{V}_{h0}^{\mathrm{el}} \subset \boldsymbol{V}_{h0}^{\mathrm{sBDFM}} \subset \boldsymbol{V}_{h0}^{\mathrm{ZZZ}}$ and $\boldsymbol{V}_{h0}^{\mathrm{el}} \subset \boldsymbol{V}_{h0}^{\mathrm{MTW}}$, which implies that $\boldsymbol{V}_{h0}^{\mathrm{el}} \subset \boldsymbol{V}_{h0}^{\mathrm{ZZZ}} \cap \boldsymbol{V}_{h0}^{\mathrm{MTW}}$. On the other hand, given $\boldsymbol{v}_h \in \boldsymbol{V}_{h0}^{\mathrm{ZZZ}} \cap \boldsymbol{V}_{h0}^{\mathrm{MTW}}$, $\boldsymbol{v}_h|_T \in \boldsymbol{P}_2(T)$, the normal component of $\boldsymbol{v}_h|_T$ is piecewise linear, and $\mathrm{div}\, \boldsymbol{v}_h|_T$ is a constant on T for any $T \in \mathscr{T}_h$; namely, $\boldsymbol{v}_h|_T \in \boldsymbol{P}^{1+}(T)$. Since all these spaces $\boldsymbol{V}_{h0}^{\mathrm{el}}$, $\boldsymbol{V}_{h0}^{\mathrm{ZZZ}}$ and $\boldsymbol{V}_{h0}^{\mathrm{MTW}}$ possess the same continuity, it holds that $\boldsymbol{V}_{h0}^{\mathrm{el}} \supset \boldsymbol{V}_{h0}^{\mathrm{ZZZ}} \cap \boldsymbol{V}_{h0}^{\mathrm{MTW}}$. □

5.1.1 Basis functions

First, we present a locally supported function $\boldsymbol{\psi}_e$ that is associated with the edge $e \in \mathscr{E}_h^i$. Given $e \in \mathscr{E}_h^i$, both ends of e could be interior or one end of e could be on the boundary.

If e has a boundary vertex (see Fig. 6a), denote $\boldsymbol{\psi}_e$ as

$$\boldsymbol{\psi}_e := \begin{cases} \dfrac{S_3}{S_3 + S_1} \boldsymbol{w}_{T_3,e_1},\ in\ T_3, \\ \boldsymbol{\eta}_{T_1,e_1,e} + \dfrac{d_1 \cos\alpha_2}{d_2} \boldsymbol{w}_{T_1,e_1,e} + \dfrac{S_3}{S_3 + S_1} \boldsymbol{w}_{T_1,e_1} - \dfrac{\tilde{S}_{\triangle(A_1,A_2,A_4)}}{S_1 + S_2} \boldsymbol{w}_{T_1,e},\ in\ T_1, \\ -\boldsymbol{\eta}_{T_2,e_4,e} + \dfrac{d_4 \cos\alpha_4}{d_3} \boldsymbol{w}_{T_2,e_4,e} + \dfrac{S_4}{S_4 + S_2} \boldsymbol{w}_{T_2,e_4} - \dfrac{\tilde{S}_{\triangle(A_1,A_2,A_4)}}{S_1 + S_2} \boldsymbol{w}_{T_2,e},\ in\ T_2, \\ \dfrac{S_4}{S_4 + S_2} \boldsymbol{w}_{T_4,e_4},\ in\ T_4. \end{cases} \tag{5.1}$$

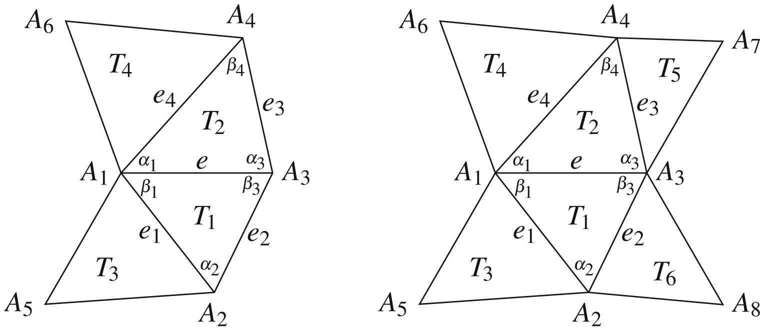

(a) $A_1 \in \mathscr{X}_h^i, A_3 \in \mathscr{X}_h^b$ **(b)** $A_1, A_3 \in \mathscr{X}_h^i$

Fig. 6 Illustration of the supports of basis functions associated with interior edges

If both of the ends of e are interior vertices (see Fig. 6b), $\boldsymbol{\psi}_e$ is denoted by

$$\boldsymbol{\psi}_e := \begin{cases} \dfrac{S_3}{2(S_3+S_1)}\boldsymbol{w}_{T_3,e_1}, \ in\ T_3, \\ \dfrac{S_4}{2(S_4+S_2)}\boldsymbol{w}_{T_4,e_4}, \ in\ T_4, \\ (\dfrac{S_3}{2(S_3+S_1)}-1)\boldsymbol{w}_{T_1,e_1}+(1-\dfrac{S_6}{2(S_6+S_1)})\boldsymbol{w}_{T_1,e_2}+\dfrac{\tilde{S}_{\triangle(A3,A4,A2)}-\tilde{S}_{\triangle(A1,A2,A4)}}{2(S_1+S_2)}\boldsymbol{w}_{T_1,e} \\ \qquad +(\dfrac{d_2\cos\beta_3}{d}-\dfrac{1}{2})\boldsymbol{w}_{T_1,e_1,e_2}+\dfrac{1}{2}\boldsymbol{w}_{T_1,e_1,e}-\dfrac{1}{2}\boldsymbol{w}_{T_1,e_2,e}+\boldsymbol{\eta}_{T_1,e_1,e_2}, \ in\ T_1, \\ (\dfrac{S_4}{2(S_4+S_2)}-1)\boldsymbol{w}_{T_2,e_4}+(1-\dfrac{S_5}{2(S_5+S_2)})\boldsymbol{w}_{T_2,e_3}+\dfrac{\tilde{S}_{\triangle(A3,A4,A2)}-\tilde{S}_{\triangle(A1,A2,A4)}}{2(S_1+S_2)}\boldsymbol{w}_{T_2,e} \\ \qquad +(\dfrac{1}{2}-\dfrac{d_4\cos\beta_1}{d})\boldsymbol{w}_{T_2,e_3,e_4}+\dfrac{1}{2}\boldsymbol{w}_{T_2,e_4,e}-\dfrac{1}{2}\boldsymbol{w}_{T_2,e_3,e}-\boldsymbol{\eta}_{T_2,e_3,e_4}, \ in\ T_2, \\ -\dfrac{S_5}{2(S_5+S_2)}\boldsymbol{w}_{T_5,e_3}, \ in\ T_5, \\ -\dfrac{S_6}{2(S_6+S_1)}\boldsymbol{w}_{T_6,e_2}, \ in\ T_6. \end{cases} \tag{5.2}$$

Remark 5.2 It is still possible that the support of a basis function associated with an interior edge can cover exactly three or five cells. These can be viewed as the degenerated cases, and the function $\boldsymbol{\psi}_e$ can be defined the same way. Specifically, when T_3 and T_4 coincide, the pattern in Fig. 6a degenerates to a patch with three cells, as shown in Fig. 7a; moreover, $\boldsymbol{\psi}_e|_{T_3} = \frac{S_3}{S_3+S_1}\boldsymbol{w}_{T_3,e_1} + \frac{S_3}{S_3+S_2}\boldsymbol{w}_{T_3,e_4}$ and $\boldsymbol{\psi}_e|_{T_i}(i=1,2)$ are the same as their counterparts in (5.1). Correspondingly, the pattern in Fig. 6b degenerates to a set of five cells, as shown in Fig. 7b; $\boldsymbol{\psi}_e|_{T_3} = \frac{S_3}{(2S_3+S_1)}\boldsymbol{w}_{T_3,e_1} + \frac{S_3}{2(S_3+S_2)}\boldsymbol{w}_{T_3,e_4}$ and $\boldsymbol{\psi}_e|_{T_i}(i=1,2,5,6)$ have the same counterparts as (5.2).

Lemma 5.3 $V_{h0}^{\mathrm{el}} = \mathrm{span}\{\boldsymbol{\psi}_e,\ e \in \mathscr{E}_h^i;\ \boldsymbol{\psi}_T,\ T \in \mathscr{T}_h^i\}.$

For completeness, we provide the proof of Lemma 5.3 in Appendix B.2.

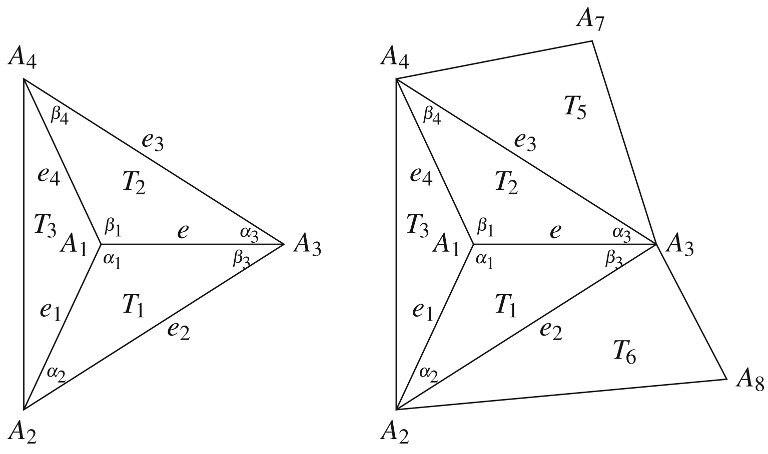

(a) $A_1 \in \mathscr{X}_h^i, A_3 \in \mathscr{X}_h^b$ **(b)** $A_1, A_3 \in \mathscr{X}_h^i$

Fig. 7 Two cases of degeneration; see Remark 5.2

5.2 A lowest-degree conservative scheme for the Stokes equation

We denote

$\mathbb{P}_h^0(\mathscr{T}_h) := \{q_h \in L^2(\Omega) : q_h|_T \in P_0(T), \forall\, T \in \mathscr{T}_h\}$, and $\mathbb{P}_{h0}^0(\mathscr{T}_h) := \mathbb{P}_h^0(\mathscr{T}_h) \cap L_0^2(\Omega)$.

Based on the new finite element, the discretization scheme of (1.3) is: Find $(\boldsymbol{u}_h, p_h) \in \boldsymbol{V}_{h0}^{\mathrm{el}} \times \mathbb{P}_{h0}^0$, such that

$$\begin{cases} \varepsilon^2\big(\nabla_h \boldsymbol{u}_h, \nabla_h \boldsymbol{v}_h\big) - (\operatorname{div} \boldsymbol{v}_h, p_h) & = (\boldsymbol{f}, \boldsymbol{v}_h), \quad \forall\, \boldsymbol{v}_h \in \boldsymbol{V}_{h0}^{\mathrm{el}}, \\ (\operatorname{div} \boldsymbol{u}_h, q_h) & = 0, \qquad\quad\; \forall\, q_h \in \mathbb{P}_{h0}^0. \end{cases} \tag{5.3}$$

Lemma 5.4 *(Stability of $\boldsymbol{V}_{h0}^{\mathrm{el}}$–$\mathbb{P}_{h0}^0$) It holds uniformly that*

$$\inf_{q_h \in \mathbb{P}_{h0}^0} \sup_{\boldsymbol{v}_h \in \boldsymbol{V}_{h0}^{\mathrm{el}}} \frac{(\operatorname{div} \boldsymbol{v}_h, q_h)}{\|q_h\|_{0,\Omega} \|\boldsymbol{v}_h\|_{1,h}} \geq C > 0.$$

Proof Given $q_h \in \mathbb{P}_{h0}^0 \subset \mathbb{P}_{h0}^1$, there exists a $\boldsymbol{v}_h \in \boldsymbol{V}_{h0}^{\mathrm{sBDFM}}$, such that $\|\boldsymbol{v}_h\|_{1,h} \leq C\|q_h\|_{0,\Omega}$ and $\operatorname{div} \boldsymbol{v}_h = q_h$, which implies $\boldsymbol{v}_h \in \boldsymbol{V}_{h0}^{\mathrm{el}}$. The proof is completed. □

Lemma 5.5 *Given $\boldsymbol{w} \in \boldsymbol{H}^2(\Omega)$, it holds that*

$$\inf_{\boldsymbol{v}_h \in \boldsymbol{V}_h^{\mathrm{el}}} \|\boldsymbol{w} - \boldsymbol{v}_h\|_{1,h} \leq Ch\|\boldsymbol{w}\|_{2,\Omega}. \tag{5.4}$$

Given $\boldsymbol{w} \in \boldsymbol{H}^2(\Omega) \cap \boldsymbol{H}_0^1(\Omega)$, such that $\operatorname{div} \boldsymbol{w} = 0$, *it holds that*

$$\inf_{\boldsymbol{v}_h \in \boldsymbol{V}_{h0}^{\mathrm{sBDFM}},\, \operatorname{div} \boldsymbol{v}_h = 0} \|\boldsymbol{w} - \boldsymbol{v}_h\|_{1,h} \leq Ch\|\boldsymbol{w}\|_{2,\Omega}. \tag{5.5}$$

Proof Since linear element space is contained in $\boldsymbol{V}_{h0}^{\mathrm{el}}$, the estimation (5.4) holds directly. Also, (5.5) follows from Lemma 3.2 and Remark 5.1. The proof is completed. □

The system (5.3) is uniformly well-posed by Brezzi's theory.

Lemma 5.6 *The problem (5.3) admits a unique solution pair* $(\boldsymbol{u}_h, p_h)$*, and it holds that*

$$\varepsilon \|\boldsymbol{u}_h\|_{1,h} + \frac{1}{\varepsilon}\|p_h\|_{0,\Omega} \eqsim \frac{1}{\varepsilon}\|\boldsymbol{f}\|_{-1,h},$$

where $\|\boldsymbol{f}\|_{-1,h} := \sup_{\boldsymbol{v}_h \in \boldsymbol{V}_{h0}^{\mathrm{el}}} \frac{(\boldsymbol{f}, \boldsymbol{v}_h)}{\|\boldsymbol{v}_h\|_{1,h}}$.

Theorem 5.1 *Let* $(\boldsymbol{u}, p)$ *and* $(\boldsymbol{u}_h, p_h)$ *be the solutions of (1.4) and (5.3), respectively. If* $\boldsymbol{u} \in \boldsymbol{H}^2(\Omega)$ *and* $p \in H^1(\Omega)$*, then*

$$\|\boldsymbol{u} - \boldsymbol{u}_h\|_{1,h} \le Ch\|\boldsymbol{u}\|_{2,\Omega}, \quad \|p - p_h\|_{0,\Omega} \le Ch(\varepsilon^2\|\boldsymbol{u}\|_{2,\Omega} + \|p\|_{1,\Omega}).$$

Here, the constant C *does not depend on the parameter* ε.

Proof The argument is standard, so we omit the details here. We only note that, as the scheme is strictly conservative, the velocity solution $\boldsymbol{u}$ can be completely separated from the pressure p, and Lemma 5.5 works here. $\square$

Remark 5.3 A further reduction of $\boldsymbol{V}_h^{\mathrm{el}}$ leads to the spaces:

$$\boldsymbol{V}_h^1 := \left\{\boldsymbol{v}_h \in \boldsymbol{H}(\mathrm{div}, \Omega) : \boldsymbol{v}_h|_T \in \boldsymbol{P}_1(T), \ \forall T \in \mathscr{T}, \ \int_e \boldsymbol{v}_h \cdot \mathbf{t} \text{ is continuous across } e \in \mathscr{E}_h^i\right\},$$

and

$$\boldsymbol{V}_{h0}^1 := \left\{\boldsymbol{v}_h \in \boldsymbol{V}_h^1 \cap \boldsymbol{H}_0(\mathrm{div}, \Omega), \ \int_e \boldsymbol{v}_h \cdot \mathbf{t} = 0 \text{ on boundary edges } e \in \mathscr{E}_h^b\right\}.$$

As it passes the patch test, the pair $\boldsymbol{V}_{h0}^1$–$\mathbb{P}_{h0}^0$ may be viewed as the most natural, if not the only, $\boldsymbol{P}_1$–P_0 pair for the Stokes problem. Generally, this pair is not stable; refer to Appendix A for a numerical verification. Accordingly, we recognize the $\boldsymbol{V}_{h0}^{\mathrm{el}}$–$\mathbb{P}_{h0}^0$ pair as a **lowest-degree** stable conservative pair for the Stokes problem on general triangulations.

6 Numerical Examples

In this section, we investigate the numerical properties of $\boldsymbol{V}_{h0}^{\mathrm{el}}$–$\mathbb{P}_{h0}^0$. In theory, the pairs $\boldsymbol{V}_{h0}^{\mathrm{sBDFM}}$–$\mathbb{P}_{h0}^1$ and $\boldsymbol{V}_{h0}^{\mathrm{el}}$–$\mathbb{P}_{h0}^0$ lead to same numerical velocity solutions on the same grids, and numerical experiments validate it. Thus we do not present separate experiments with respect to $\boldsymbol{V}_{h0}^{\mathrm{sBDFM}}$–$\mathbb{P}_{h0}^1$. All simulations are performed on uniformly refined grids.

It has been revealed that $\boldsymbol{V}_{h0}^{\mathrm{el}}$ does not correspond to a Ciarlet's triple. However, it does admit a set of tightly supported basis functions. This makes the $\boldsymbol{V}_{h0}^{\mathrm{el}}$–$\mathbb{P}_{h0}^0$ embedded in the standard framework of programming. Precisely, on every cell, only a fixed small number (no more than 13) of basis functions contribute to the cell-wise stiffness matrix, and the assembly of cell-wise stiffness matrices into a global stiffness matrix follows the standard procedure. The numerical experiments given verify the implementability of the scheme.

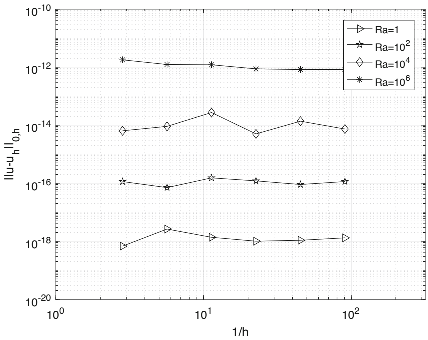

(a) L^2-norm

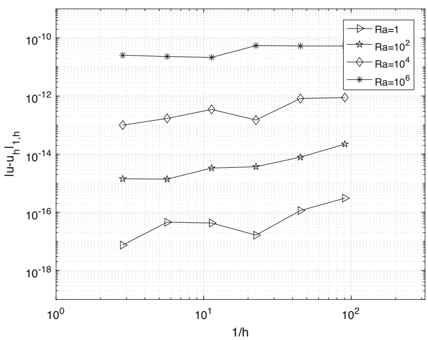

(b) H^1-norm

Fig. 8 Velocity errors in the no-flow Stokes equations by the $\boldsymbol{P}^{1+} - P_0$ pair

6.1 On the pressure robustness with respect to parameter *Ra*

This example was introduced in [22]. Here, we utilize it to show that the pair $\boldsymbol{P}^{1+}$–P_0 is of pressure robustness. Consider the Stokes Eq. (1.3) in $\Omega = (0, 1) \times (0, 1)$ with $\varepsilon = 1$ and $\boldsymbol{f} = (0, Ra(1 - y + 3y^2))^T$, where $Ra > 0$ is a parameter. The exact solution pair is $\boldsymbol{u} = 0$ and $p = Ra(y^3 - 2/y^2 + y - 7/12)$. For the continuous problem, changing the parameter Ra in the right-hand side changes only the pressure. It was suggested in [22] that for standard finite elements, the discrete velocity is far from being equal to zero even for $Ra = 1$. However, as is shown in Fig. 8, for the new pair $\boldsymbol{V}_{h0}^{\mathrm{el}}$–$\mathbb{P}_{h0}^{0}$, the numerical velocities are close to zero for different values of Ra, which implies the pair's pressure robustness with respect to the parameter Ra.

6.2 On the ε−robustness

This example is designed to test ε robustness with fixed $\boldsymbol{f}$. Consider the Stokes problem (1.3) in $\Omega = (0, 1) \times (0, 1)$. Assume $\varepsilon = 1$ and the exact solution pair $(\boldsymbol{u}, p) = (\boldsymbol{u}^{\varepsilon=1}, p^{\varepsilon=1})$ with $\boldsymbol{u}^{\varepsilon=1} = \mathrm{curl}(\frac{1}{2}x^2y^2(x-1)^2(y-1)^2)$ and $p^{\varepsilon=1} = 3x^2 + 3y^2 - 2$. Consequently we obtain $\boldsymbol{f}^{\varepsilon=1}$. Now, for the continuous problem (1.3) with $p = p^{\varepsilon=1}$ and $\boldsymbol{f} = \boldsymbol{f}^{\varepsilon=1}$ fixed, changing ε only changes the true velocity solution to $\frac{1}{\varepsilon^2}\boldsymbol{u}^{\varepsilon=1} =: \boldsymbol{u}^{\varepsilon}$, while $p^{\varepsilon} = p^{\varepsilon=1}$. For the discrete problem (5.3), we still hope to find this law. We denote $(\boldsymbol{u}_h^{\varepsilon=1}, p_h^{\varepsilon=1})$ and $(\boldsymbol{u}_h^{\varepsilon}, p_h^{\varepsilon})$ as numerical solutions associated with $(\boldsymbol{u}^{\varepsilon=1}, p^{\varepsilon=1})$ and $(\boldsymbol{u}^{\varepsilon}, p^{\varepsilon})$, respectively. Numerical tests show that $\boldsymbol{u}_h^{\varepsilon} = \frac{1}{\varepsilon^2}\boldsymbol{u}_h^{\varepsilon=1}$ and $p_h^{\varepsilon} = p_h^{\varepsilon=1}$. For the convenience of display, we present the errors of velocity below:

It can be observed that

(i) when the mesh level is fixed, both $\|\boldsymbol{u}^{\varepsilon} - \boldsymbol{u}_h^{\varepsilon}\|_{0,h}$ and $|\boldsymbol{u}^{\varepsilon} - \boldsymbol{u}_h^{\varepsilon}|_{1,h}$ are of the $\mathscr{O}((\frac{1}{\varepsilon})^2)$ order, while $\|p^{\varepsilon} - p_h^{\varepsilon}\|_{0,h}$ is of the $\mathscr{O}((\frac{1}{\varepsilon})^0)$ order; this corresponds to our expectation;
(ii) when ε is fixed, velocity errors in the L^2-norm and H^1-norm are of the $\mathscr{O}(h^2)$ and $\mathscr{O}(h)$ order, respectively, and pressure errors are of the $\mathscr{O}(h)$ order.

Table 1 Errors of velocity in the L^2-norm by the $\boldsymbol{P}^{1+} - P_0$ pair

$\varepsilon \setminus$ mesh	0	1	2	3	4	5
2^0	1.1842e-03	3.1055e-04	7.7790e-05	1.9423e-05	4.8543e-06	1.2138e-06
2^{-2}	1.8948e-02	4.9687e-03	1.2446e-03	3.1076e-04	7.7668e-05	1.9421e-05
2^{-4}	3.0316e-01	7.9500e-02	1.9914e-02	4.9722e-03	1.2427e-03	3.1073e-04
2^{-6}	4.8506e+00	1.2720e+00	3.1863e-01	7.9556e-02	1.9883e-02	4.9717e-03
2^{-8}	7.7610e+01	2.0352e+01	5.0980e+00	1.2729e+00	3.1813e-01	7.9548e-02
2^{-10}	1.2418e+03	3.2563e+02	8.1569e+01	2.0366e+01	5.0901e+00	1.2728e+00

Table 2 Errors of velocity in the H^1-norm by the $\boldsymbol{P}^{1+} - P_0$ pair

$\varepsilon \setminus$ mesh	0	1	2	3	4	5
2^0	1.6547e-02	8.3712e-03	4.1852e-03	2.0904e-03	1.0448e-03	5.2232e-04
2^{-2}	2.6476e-01	1.3394e-01	6.6963e-02	3.3446e-02	1.6716e-02	8.3571e-03
2^{-4}	4.2361e+00	2.1430e+00	1.0714e+00	5.3514e-01	2.6746e-01	1.3371e-01
2^{-6}	6.7778e+01	3.4288e+01	1.7142e+01	8.5623e+00	4.2793e+00	2.1394e+00
2^{-8}	1.0844e+03	5.4862e+02	2.7428e+02	1.3700e+02	6.8469e+01	3.4231e+01
2^{-10}	1.7351e+04	8.7778e+03	4.3885e+03	2.1919e+03	1.0955e+03	5.4769e+02

6.3 On the convergence in polygon regions (with unstructured subdivisions)

In this subsection, simulations for Stokes problems are performed in various domains with general triangulations to verify the convergence rate results in Theorem 5.1 for finite element approximation $\boldsymbol{V}_{h0}^{\mathrm{el}}$–$\mathbb{P}_{h0}^0$.

Consider the Stokes problem (1.3) in the two-dimensional domain Ω, which is sequentially a rectangle, a hexagon, a pentagon, an L-shaped area, and a star-shaped area.

For each domain, we denote $\partial\Omega = \cup_i \Gamma_i$. Also, we define $\phi = C_\phi \prod_{\Gamma_i \subset \partial\Omega} (r(\Gamma_i))^2$, with $r(\Gamma_i) = 0$ representing the equation of Γ_i; for the precise expression of $r(\Gamma_i)$, refer to each example's caption. Assume $\varepsilon = 1$, and the right-hand side $\boldsymbol{f}$ is chosen such that the exact solution pair is $\boldsymbol{u} = \mathrm{curl}\,\phi$ and $p = 3x^2 + 3y^2 + C_p$, where C_p satisfies $\int_\Omega p\,dx = 0$.

For every test, we display the domains with the initial grid in the left, and corresponding error convergence figures are given on the right (Figs. 9, 10, 11, 12 and 13).

From these examples, the convergence rate of the velocity is approximately two with respect to the L^2-norm and one to H^1-norm; the convergence rate of the pressure is approximately one with respect to the L^2-norm; these are consistent with the analysis in Theorem 5.1.

7 Concluding Remarks

In this study, a new conservative pair, $\boldsymbol{V}_{h0}^{\mathrm{el}}$–$\mathbb{P}_{h0}^0$, is established and shown to be stable for the incompressible Stokes problem, and a numerical verification (see Appendix A) illustrates that the $\boldsymbol{V}_{h0}^{\mathrm{el}}$–$\mathbb{P}_{h0}^0$ pair is the lowest-degree one that is stable and conservative on general triangulations. The velocity component, in a generalized sense, can also be viewed as the

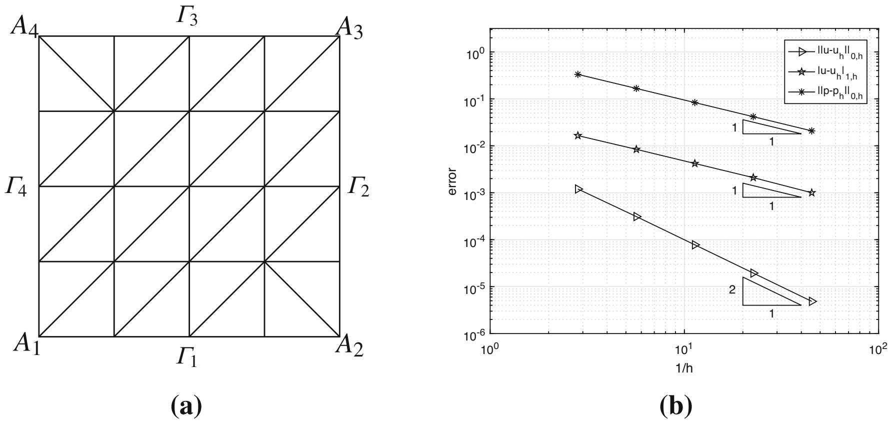

Fig. 9 *Example 1*. Left: An initially divisioned unit square domain, with $\partial\Omega = \cup_{i=1}^{4}\Gamma_i$, $A_1(0,0)$, $A_2(1,0)$, $A_3(1,1)$, and $A_4(0,1)$; Right: Velocity errors in the L^2- and H^1-norm and pressure errors in the L^2-norm by the $\boldsymbol{P}^{1+} - P_0$ pair, with $r(\Gamma_1) = y$, $r(\Gamma_2) = x - 1$, $r(\Gamma_3) = y - 1$, $r(\Gamma_4) = x$, $C_p = -2$, and $C_\phi = 1/2$

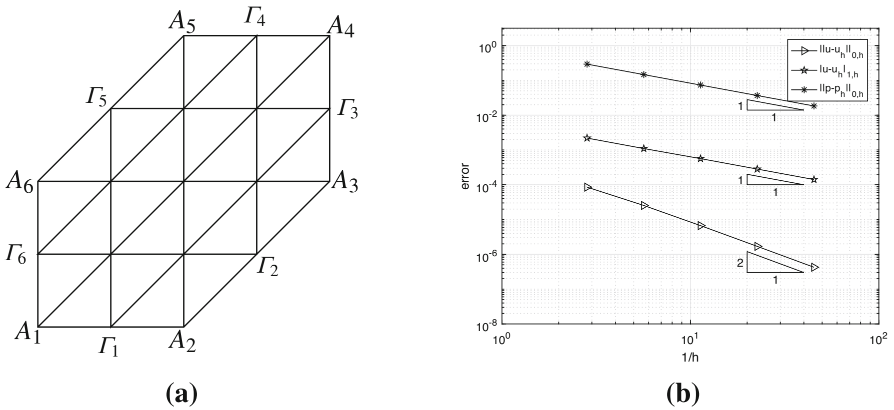

Fig. 10 *Example 2*. Left: An initially divisioned hexagon domain, with $\partial\Omega = \cup_{i=1}^{6}\Gamma_i$, $A_1(0,0)$, $A_2(0.5,0)$, $A_3(1,0.5)$, $A_4(1,1)$, $A_5(0.5,1)$, and $A_6(0,0.5)$; Right: Velocity errors in the L^2- and H^1-norm and pressure errors in the L^2-norm by the $\boldsymbol{P}^{1+} - P_0$ pair, with $r(\Gamma_1) = y$, $r(\Gamma_2) = 2x - 2y - 1$, $r(\Gamma_3) = x - 1$, $r(\Gamma_4) = y - 1$, $r(\Gamma_5) = 2x - 2y + 1$, $r(\Gamma_6) = x$, $C_p = -23/12$, and $C_\phi = 1/16$

$H(\mathrm{div})$ element functions added with piecewise divergence-free normal-bubble functions, and is thus comparable with ones given in, for example, [14, 25, 35]. However, the finite element space for velocity does not correspond to a Ciarlet's triple, and the construction and theoretical analysis cannot be carried out in the usual way. The main technical ingredient is thus to use an indirect approach by constructing and utilizing the auxiliary pair $\boldsymbol{V}_{h0}^{\mathrm{sBDFM}}$–$\mathbb{P}_{h0}^{1}$.

The auxiliary pair $\boldsymbol{V}_{h0}^{\mathrm{sBDFM}}$–$\mathbb{P}_{h0}^{1}$ is constructed by reducing $H(\mathrm{div})$ finite element spaces, as adopted in [37]. Note that the sBDFM element has the same nodal functionals as ones given in [25, 35] and [14] (the lowest-degree one of each), but it uses the lowest-degree polynomials among these four, and only the sBDFM element space can accompany the piecewise linear polynomial space to form a stable pair. The other three can only accompany the piecewise constant space.

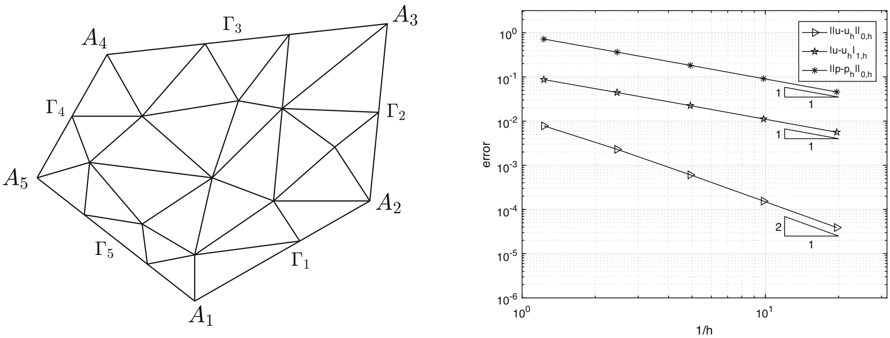

(a) **(b)**

Fig. 11 *Example 3.* Left: An initially divisioned pentagon domain, with $\partial\Omega = \cup_{i=1}^{5}\Gamma_i$, $A_1(-0.1, -0.8)$, $A_2(0.9, -0.15)$, $A_3(1, 1)$, $A_4(-0.6, 0.8)$, and $A_5(-1, 0)$; Right: Velocity errors in the L^2- and H^1-norm and pressure errors in the L^2-norm by the $\boldsymbol{P}^{1+} - P_0$ pair, with $r(\Gamma_1) = 130x - 200y - 147$, $r(\Gamma_2) = 23x - 2y - 21$, $r(\Gamma_3) = x - 8y + 7$, $r(\Gamma_4) = 2x - y + 2$, $r(\Gamma_5) = 8x + 9y + 8$, $C_p = -205333/153120$, and $C_\phi = 10^{-13}$

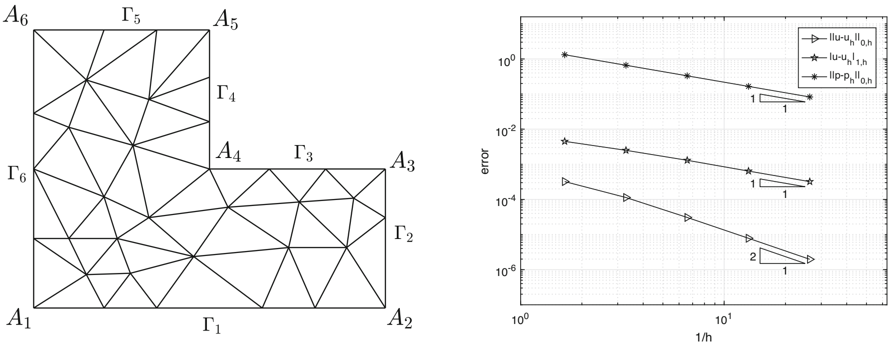

(a) **(b)**

Fig. 12 *Example 4.* Left: An initially divisioned L-shaped domain with $\partial\Omega = \cup_{i=1}^{6}\Gamma_i$, $A_1(0, 0)$, $A_2(2, 0)$, $A_3(2, 1)$, $A_4(1, 1)$, $A_5(1, 2)$, and $A_6(0, 2)$; Right: Velocity errors in the L^2- and H^1-norm and pressure errors in the L^2-norm by the $\boldsymbol{P}^{1+} - P_0$ pair, with $r(\Gamma_1) = y$, $r(\Gamma_2) = x - 2$, $r(\Gamma_3) = y - 1$, $r(\Gamma_4) = x - 1$, $r(\Gamma_5) = y - 2$, $r(\Gamma_6) = x$, $C_p = -6$, and $C_\phi = 10^{-2}$

As for conservative pairs in three-dimension, we refer to [16, 40, 44], where composite grids were required, as well as [17] and [43], where high-degree local polynomials were utilized. We refer to [8, 21, 42] for pairs on rectangular grids and [26] for ones on cubic grids, where full advantage was taken of the geometric symmetry of the cells. The approaches given in [37] and the present paper can be generalized to higher dimensions and non-simplicial grids. This will be discussed in the future.

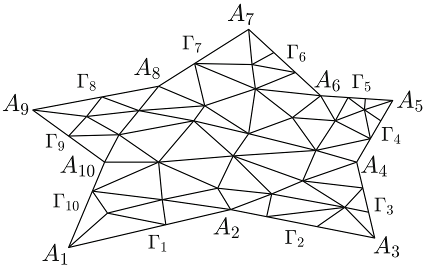

(a)

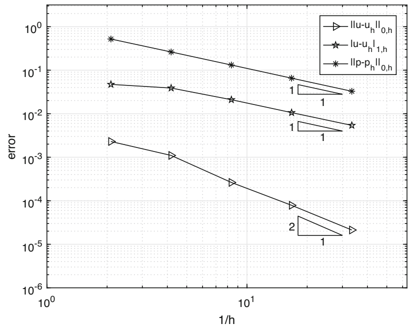

(b)

Fig. 13 *Example 5.* Left: An initially divisioned star-shape domain, with $\partial\Omega = \cup_{i=1}^{10}\Gamma_i$, $A_1(-1,-1.2)$, $A_2(-0.1,-0.8)$, $A_3(0.7,-1.1)$, $A_4(0.6,-0.3)$, $A_5(0.8,0.35)$, $A_6(0.4,0.4)$, $A_7(0,1.1)$, $A_8(-0.5,0.5)$, $A_9(-1.2,0.25)$, and $A_{10}(-0.8,-0.3)$; Right: Velocity errors in the L^2- and H^1-norm and pressure errors in the L^2-norm by the $\boldsymbol{P}^{1+} - P_0$ pair, with $r(\Gamma_1) = 20x - 45y - 34$, $r(\Gamma_2) = 30x + 80y + 67$, $r(\Gamma_3) = 16x + 2y - 9$, $r(\Gamma_4) = 13x - 4y - 9$, $r(\Gamma_5) = 5x + 40y - 18$, $r(\Gamma_6) = 35x + 20y - 22$, $r(\Gamma_7) = 12x - 10y + 11$, $r(\Gamma_8) = 10x - 28y + 19$, $r(\Gamma_9) = 55x + 40y + 56$, $r(\Gamma_{10}) = 45x - 10y + 33$, $C_p = -243923/163680$, and $C_\phi = 10^{-30}$

Acknowledgements The authors would like to thank the anonymous referees for their valuable comments and suggestions.

Funding The research is supported by NSFC (No. 11871465) and CAS (No. XDB41000000). The authors have no relevant financial or non-financial interests to disclose. The work has no associated data.

Data Availability Enquiries about data availability should be directed to the authors.

Declarations

Conflict of interest The authors have not disclosed any competing interests.

Appendix

A The Most Natural Linear–Constant Pair is not Stable: A Numerical Verification

In this section, we show by numerics the pair, $\boldsymbol{V}_{h0}^1$–$\mathbb{P}_{h0}^0$, defined in Remark 5.3, is not stable on general triangulations, whereas

$$\inf_{q_h \in \operatorname{div} \boldsymbol{V}_{h0}^1} \sup_{\boldsymbol{v}_h \in \boldsymbol{V}_{h0}^1} \frac{(\operatorname{div} \boldsymbol{v}_h, q_h)}{\|q_h\|_{0,\Omega} |\boldsymbol{v}_h|_{1,h}} = \mathscr{O}(h) \tag{A.1}$$

on a specific kind of triangulations.

A.1 A special triangulation and finite element space

We consider the computational domain $\Omega = (0,1)\times(0,1)\setminus(\{(x,y): 0 \le x \le \frac{1}{2}, x+\frac{1}{2} \le y \le 1\} \cup \{(x,y): \frac{1}{2} \le x \le 1, 0 \le y \le x-\frac{1}{2}\})$. The initial triangulation is shown in Fig. 14a, and a sequence of triangulations is obtained by refining it uniformly (cf. Fig. 14b).

Given a patch P_A as shown in Fig. 14a, we denote $\boldsymbol{V}_{h0}^1(P_A) = \text{span}\{\boldsymbol{\varphi}_1^A, \boldsymbol{\varphi}_2^A, \boldsymbol{\varphi}_3^A\}$, and for $i = 1:6$, $\boldsymbol{V}_{h0}^1(T_i) = \text{span}\{\boldsymbol{\varphi}_{T_i}^1, \boldsymbol{\varphi}_{T_i}^2, \boldsymbol{\varphi}_{T_i}^3\}$. Specifically, for $s = 1:2$, $i = 1:6$, $\boldsymbol{\varphi}_s^A|_{T_i} = \boldsymbol{\varphi}_{T_i}^s$, and for $s = 3$,

$$\boldsymbol{\varphi}_3^A = \begin{cases} \boldsymbol{\varphi}_{T_1}^1 - 2\boldsymbol{\varphi}_{T_1}^2 + \boldsymbol{\varphi}_{T_1}^3,\ in\ T_1; & \boldsymbol{\varphi}_{T_2}^1 - \boldsymbol{\varphi}_{T_2}^2 - \boldsymbol{\varphi}_{T_2}^3,\ in\ T_2; \\ 2\boldsymbol{\varphi}_{T_3}^1 - \boldsymbol{\varphi}_{T_3}^2 + \boldsymbol{\varphi}_{T_3}^3,\ in\ T_3; & \boldsymbol{\varphi}_{T_4}^1 - 2\boldsymbol{\varphi}_{T_4}^2 + \boldsymbol{\varphi}_{T_4}^3,\ in\ T_4; \\ \boldsymbol{\varphi}_{T_5}^1 - \boldsymbol{\varphi}_{T_5}^2 - \boldsymbol{\varphi}_{T_5}^3,\ in\ T_5; & 2\boldsymbol{\varphi}_{T_6}^1 - \boldsymbol{\varphi}_{T_6}^2 + \boldsymbol{\varphi}_{T_6}^3,\ in\ T_6; \end{cases}$$

where for $i = 1:6$, $\boldsymbol{\varphi}_{T_i}^1 = \begin{pmatrix} \lambda \\ 0 \end{pmatrix}$, $\boldsymbol{\varphi}_{T_i}^2 = \begin{pmatrix} 0 \\ \lambda \end{pmatrix}$, and $\boldsymbol{\varphi}_{T_1}^3 = \begin{pmatrix} \lambda_6 - \lambda_1 \\ 0 \end{pmatrix}$, $\boldsymbol{\varphi}_{T_2}^3 = \begin{pmatrix} \lambda_1 - \lambda_2 \\ \lambda_1 - \lambda_2 \end{pmatrix}$, $\boldsymbol{\varphi}_{T_3}^3 = \begin{pmatrix} 0 \\ \lambda_2 - \lambda_3 \end{pmatrix}$, $\boldsymbol{\varphi}_{T_4}^3 = \begin{pmatrix} \lambda_3 - \lambda_4 \\ 0 \end{pmatrix}$, $\boldsymbol{\varphi}_{T_5}^3 = \begin{pmatrix} \lambda_4 - \lambda_5 \\ \lambda_4 - \lambda_5 \end{pmatrix}$, $\boldsymbol{\varphi}_{T_6}^3 = \begin{pmatrix} 0 \\ \lambda_5 - \lambda_6 \end{pmatrix}$.

Similarly to Lemma 4.3, we can show the lemma below:

Lemma A.1 $dim(\boldsymbol{V}_{h0}^1) = 3\#\mathscr{X}_h^i$ *and* $\boldsymbol{V}_{h0}^1 = \text{span}\{\boldsymbol{\varphi}_1^A, \boldsymbol{\varphi}_2^A, \boldsymbol{\varphi}_3^A, A \in \mathscr{X}_h^i\}$.

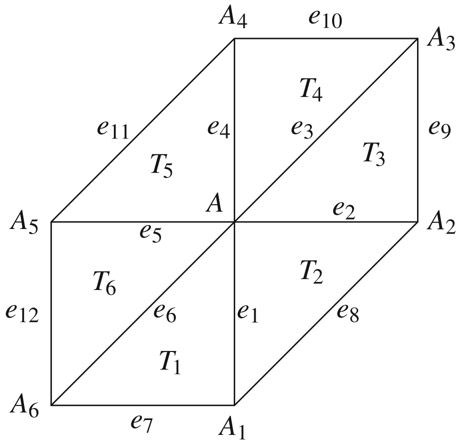

(a) an initial grid with six cells

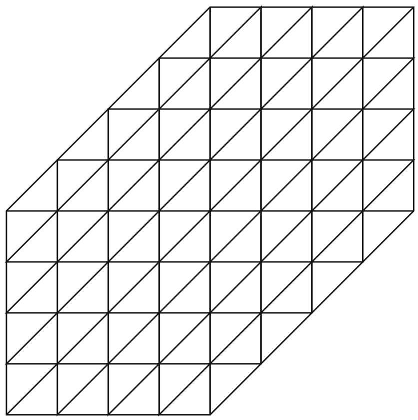

(b) a grid after twice refinements

Fig. 14 An initially divisioned grid and its sketch map after uniform refinements

A.2 Numerical Verification of the Inf-sup Constant

By the Courant's min-max theorem, it is easy to show the lemma below:

Lemma A.2 *With respect to any set of basis functions of $\boldsymbol{V}_{h0}^1$ and $\mathbb{P}_h^0$, denote by A the stiffness matrix of $(\nabla_h \cdot, \nabla_h \cdot)$ on $\boldsymbol{V}_{h0}^1$, by M the mass matrix of $(\cdot,\cdot)$ on $\boldsymbol{V}_{h0}^1$, and by B the stiffness matrix of $(\mathrm{div}\,\cdot,\cdot)$ on $\boldsymbol{V}_{h0}^1 \times \mathbb{P}_h^0$. Then*

$$\inf_{q_h \in \mathrm{div}\, \boldsymbol{V}_{h0}^1} \sup_{\boldsymbol{v}_h \in \boldsymbol{V}_{h0}^1} \frac{(\mathrm{div}\, \boldsymbol{v}_h, q_h)}{\|q_h\|_{0,\Omega} |\boldsymbol{v}_h|_{1,h}} = \lambda_{\min}^+,$$

where $\lambda_{\min}^+$ is the smallest positive eigenvalue of the matrix eigenvalue problem

$$BA^{-1}B^T \mathrm{v} = \lambda M \mathrm{v}. \tag{A.2}$$

The maximum eigenvalue of the eigenvalue problem (A.2) is denoted by $\lambda_{\max}$. Table 3 displays the computed values of $\lambda_{\min}^+$ and $\lambda_{\max}$ on a series of refined grids. Figure 15 illustrates that $\lambda_{\min}^+$ degenerates in the rate of $\mathcal{O}(h)$. This verifies (A.1) numerically.

Table 3 Computed values of $\lambda_{\min}^+$ and $\lambda_{\max}$

h	$\lambda_{\min}^+$	Rate	$\lambda_{\max}$
1/2	0.2232	–	1.3822
1/4	0.1235	0.8538	1.4081
1/8	0.0636	0.9574	1.4131
1/16	0.0321	0.9865	1.4140
1/32	0.0161	0.9955	1.4142
1/64	0.0081	0.9911	1.4142

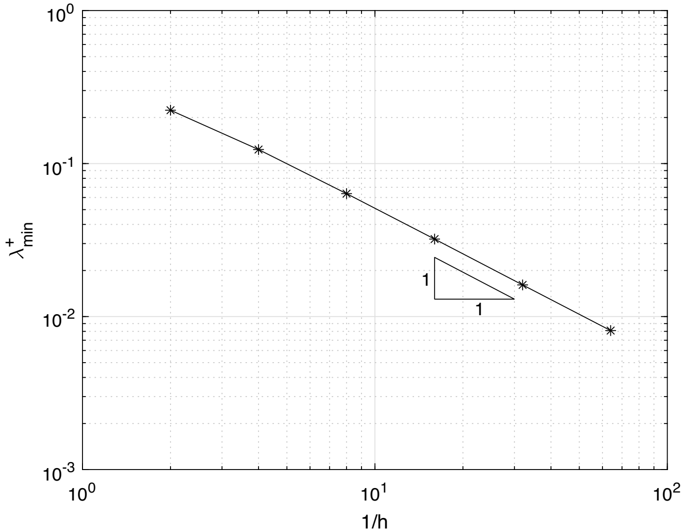

Fig. 15 λ_{min}^+ decays along with mesh refinements

B Proofs of Lemmas 4.3 and 5.3

B.1 Proof of Lemma 4.3

In this subsection, we provide the proof of Lemma 4.3, which establishes a basis of $\mathbf{Z}_{h0}$. To this end, we need to analyze $\mathbf{Z}_{h0}|_T$ with $T \in \mathscr{T}_h$ firstly.

For the interior cell $T \in \mathscr{T}_h^i$ with vertices $A_i, i = 1:3$, and neighboring cells $T_j, j = 1:3$, it is covered by functions of the set $\boldsymbol{\Psi}_h(T) = \{\boldsymbol{\psi}^{A_1}|_T, \boldsymbol{\psi}^{A_2}|_T, \boldsymbol{\psi}^{A_3}|_T, \boldsymbol{\psi}_T|_T, \boldsymbol{\psi}_{T_1}|_T, \boldsymbol{\psi}_{T_2}|_T, \boldsymbol{\psi}_{T_3}|_T\}$;see Fig. 16 for an illustration. It is clear that the seven functions in $\boldsymbol{\Psi}_h(T)$ are linearly dependent; however, any six of them are linearly independent. For conciseness, a particular case is stated in the following lemma, which also serves Lemma 4.3.

Lemma B.1 *For the interior cell $T \in \mathscr{T}_h^i$, with vertices A_i, $i = 1:3$ and neighboring cells T_j, $j = 1:3$ (see* Fig. 16 *for an illustration), the functions in $\{\boldsymbol{\psi}^{A_2}|_T, \boldsymbol{\psi}^{A_3}|_T, \boldsymbol{\psi}_T|_T, \boldsymbol{\psi}_{T_1}|_T, \boldsymbol{\psi}_{T_2}|_T, \boldsymbol{\psi}_{T_3}|_T\}$ are linearly independent.*

Proof With the help of (4.3) and (4.4), a direct calculation leads to

$$\left(\boldsymbol{\psi}^{A_2}|_T, \boldsymbol{\psi}^{A_3}|_T, \boldsymbol{\psi}_T|_T, \boldsymbol{\psi}_{T_1}|_T, \boldsymbol{\psi}_{T_2}|_T, \boldsymbol{\psi}_{T_3}|_T\right)^\top$$
$$= \mathbf{A}\left(\boldsymbol{w}_{T,e_2,e_3}, \boldsymbol{w}_{T,e_3,e_1}, \boldsymbol{w}_{T,e_1,e_2}, \boldsymbol{w}_{T,e_1}, \boldsymbol{w}_{T,e_2}, \boldsymbol{w}_{T,e_3}\right)^\top,$$
$$\text{with } \mathbf{A} = \begin{bmatrix} 0 & 1 & 0 & \frac{d_2 d_5 \sin(\alpha_3+\gamma_3)}{2(S_1+S)} & 0 & \frac{d_2 d_8 \sin(\alpha_1+\beta_1)}{2(S_3+S)} \\ 0 & 0 & 1 & \frac{d_3 d_4 \sin(\alpha_2+\beta_2)}{2(S_1+S)} & \frac{d_3 d_7 \sin(\alpha_1+\gamma_1)}{2(S_2+S)} & 0 \\ \frac{1}{3} & \frac{1}{3} & \frac{1}{3} & \frac{S_1-2S}{3(S_1+S)} & \frac{S_2-2S}{3(S_2+S)} & \frac{S_3-2S}{3(S_3+S)} \\ 0 & 0 & 0 & \frac{S}{S_1+S} & 0 & 0 \\ 0 & 0 & 0 & 0 & \frac{S}{S_2+S} & 0 \\ 0 & 0 & 0 & 0 & 0 & \frac{S}{S_3+S} \end{bmatrix}.$$

As $\det(\mathbf{A}) = \frac{1}{3}\prod_{i=1:3}\frac{S}{S+S_i} \neq 0$ and $\left\{\boldsymbol{w}_{T,e_2,e_3}, \boldsymbol{w}_{T,e_3,e_1}, \boldsymbol{w}_{T,e_1,e_2}, \boldsymbol{w}_{T,e_1}, \boldsymbol{w}_{T,e_2}, \boldsymbol{w}_{T,e_3}\right\}$ are linearly independent, it concludes that $\left\{\boldsymbol{\psi}^{A_2}|_T, \boldsymbol{\psi}^{A_3}|_T, \boldsymbol{\psi}_T|_T, \boldsymbol{\psi}_{T_1}|_T, \boldsymbol{\psi}_{T_2}|_T, \boldsymbol{\psi}_{T_3}|_T\right\}$ are linearly independent. □

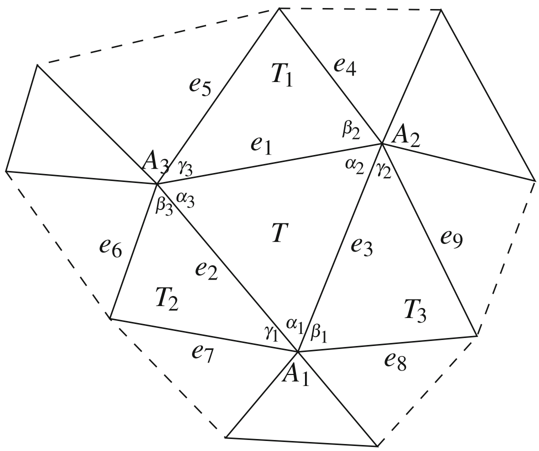

Fig. 16 Illustration of the supports of all kernel basis functions upon one cell

Remark B.1 If a cell $T \in \mathscr{T}_h$ has one (or more) vertices aligned on the boundary, then it is covered by no more than two interior vertex patches and contained in the supports of no more than six vertex- or cell-related kernel basis functions; the restriction of these six functions on T is linearly independent.

Proof of Lemma 4.3 We only have to prove that the functions of $\Phi_h(\mathscr{T}_h)$ are linearly independent. Indeed, provided that the set $\Phi_h(\mathscr{T}_h)$ is linearly independent, $\dim(\mathrm{span}(\Phi_h(\mathscr{T}_h))) = \#\mathscr{X}_h^i + \#\mathscr{T}_h^i = 3\#\mathscr{X}_h^i - 2 = 3\#\mathscr{E}_h^i - (3\#\mathscr{T}_h - 1) = \dim(\boldsymbol{V}_{h0}^{\mathrm{sBDFM}}) - \dim(\mathbb{P}_{h0}^1) = \dim(\boldsymbol{V}_{h0}^{\mathrm{sBDFM}}) - \dim(\mathrm{div}\,\boldsymbol{V}_{h0}^{\mathrm{sBDFM}}) = \dim(\boldsymbol{Z}_{h0})$, and thus $\boldsymbol{Z}_{h0} = \mathrm{span}\,(\Phi_h(\mathscr{T}_h))$.

Now, given $\boldsymbol{\psi}_h = \sum_{A\in\mathscr{X}_h^i} c_A\boldsymbol{\psi}^A + \sum_{T\in\mathscr{T}_h^i} c_T\boldsymbol{\psi}_T = 0$, we show that all c_A and c_T are zero. Similar to [46], we adopt a sweeping process here. Given $a \in \mathscr{X}_h^b$, let T be such that a is a vertex of T. Then,

$$\boldsymbol{\psi}_h|_T = \sum_{A\in\mathscr{X}_h^i\cap\overline{T}} c_A\boldsymbol{\psi}^A|_T + \sum_{T'\in\mathscr{T}_h^i, T' \text{ and } T \text{ share a common edge}} c_{T'}\boldsymbol{\psi}_{T'}|_T = 0.$$

By Lemma B.1 and Remark B.1, $c_A = 0$ for $A \in \mathscr{X}_h^i \cap \overline{T}$ and $c_{T'} = 0$ for $T' \in \mathscr{T}_h^i$, where T' and T share a common edge. Therefore, $c_A = 0$ for any vertex $A \in \mathscr{X}_h^i$ that is connected to one boundary vertex $a \in \mathscr{X}_h^b$, and $c_T = 0$ for any $T \in \mathscr{T}_h^i$ that connects to a boundary vertex $a \in \mathscr{X}_h^b$. Similarly, we can show

$$c_A = 0\ \forall\, A \in \mathscr{X}_h^{b,+2}, \quad c_T = 0\ \forall\, T \in \mathscr{T}_h \text{ that connects to } \mathscr{X}_h^{b,+1}.$$

Repeating the procedure recursively, finally, we obtain

$$c_A = 0\ \forall\, A \in \mathscr{X}_h^{b,+k}, \quad c_T = 0\ \forall\, T \in \mathscr{T}_h \text{ that connects to } \mathscr{X}_h^{b,+(k-1)}$$

where k is the number of levels of the triangulation $\mathscr{T}_h$. Therefore, c_A and c_T are all zero, and the functions of $\Phi_h(\mathscr{T}_h)$ are linearly independent. The proof is completed. □

B.2 Proof of Lemma 5.3

In this subsection, we provide the proof of Lemma 5.3, which establishes a basis of $\boldsymbol{V}_{h0}^{\mathrm{el}}$.

Proof of Lemma 5.3 Evidently, $\boldsymbol{V}_{h0}^{\mathrm{el}} \supset \mathrm{span}\{\boldsymbol{\psi}_e,\ e \in \mathscr{E}_h^i;\ \boldsymbol{\psi}_T,\ T \in \mathscr{T}_h^i\}$. So we turn to the other direction.

First, we show $\mathrm{span}\{\mathrm{div}\,\boldsymbol{\psi}_e,\ e \in \mathscr{E}_h^i\} = \mathbb{P}_{h0}^0$. For both cases, as in Fig. 6, $\mathrm{div}\,\boldsymbol{\psi}_e = \frac{1}{S_1}$ on T_1 and $-\frac{1}{S_2}$ on T_2, and vanishes on all the other cells. A simple algebraic argument leads to this assertion.

Second, all functions of $\boldsymbol{Z}_{h0}$ can be represented by these functions. We only have to verify it for any kernel function, which is supported in a vertex patch. □

In fact, for an interior vertex A, $P_A = \cup_{i=1:m}T_i$, $\overline{T}_i \cap \overline{T}_{i+1} = e_i$, $T_{m+1} = T_1$ and e_i connects A and A_i. Denote for $i = 1 : m$ (see Fig. 17)

$$\boldsymbol{\psi}_{e_i}^* = \begin{cases} \boldsymbol{\psi}_{e_i}, & A_i \in \mathscr{X}_h^b, \\ \boldsymbol{\psi}_{e_i} + \frac{1}{2}\boldsymbol{\psi}_{T_i} + \frac{1}{2}\boldsymbol{\psi}_{T_{i+1}}, & A_i \in \mathscr{X}_h^i. \end{cases}$$

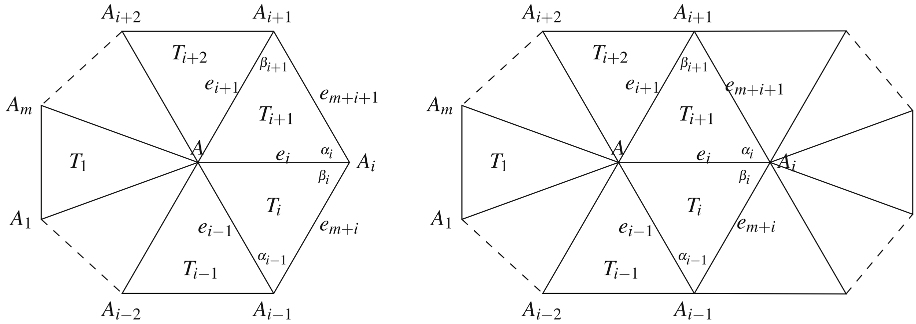

(a) $A_i \in \mathscr{X}_h^b$ **(b)** $A_i \in \mathscr{X}_h^i$

Fig. 17 Illustration of the support of $\boldsymbol{\psi}_{e_i}$. Left: e_i has one interior vertex; Right: e_i has two interior vertices

We refer to (4.3), (4.4), (5.1), (5.2) for the expressions of $\boldsymbol{\psi}^A$, $\boldsymbol{\psi}_{T_i}$ and $\boldsymbol{\psi}_{e_i}$(cf Figs. 5, 6 and 7). Then, in any event $\operatorname{supp}(\boldsymbol{\psi}^*_{e_i}) = T_{i-1} \cup T_i \cup T_{i+1} \cup T_{i+2} \subset P_A$, and $\operatorname{div} \sum_{i=1:m} \boldsymbol{\psi}^*_{e_i} = 0$. Thus $\sum_{i=1:m} \boldsymbol{\psi}^*_{e_i} \in \boldsymbol{Z}_A = \operatorname{span}\{\boldsymbol{\psi}^A\}$. A further calculation gives $\sum_{i=1:m} \boldsymbol{\psi}^*_{e_i} = \boldsymbol{\psi}^A$, which thus leads to

$$\boldsymbol{\psi}^A = \sum_{i=1:m} \boldsymbol{\psi}_{e_i} + \frac{1}{2} \sum_{i=1:m,\ A_i \in \mathscr{X}_h^i} (\boldsymbol{\psi}_{T_i} + \boldsymbol{\psi}_{T_{i+1}}).$$

Now, $\boldsymbol{V}_{h0}^{\mathrm{el}}$ and $\operatorname{span}\{\boldsymbol{\psi}_e,\ e \in \mathscr{E}_h^i;\ \boldsymbol{\psi}_T,\ T \in \mathscr{T}_h^i\}$ have the same range under the operator div. It also holds that $\boldsymbol{Z}_{h0} \subset \operatorname{span}\{\boldsymbol{\psi}_e,\ e \in \mathscr{E}_h^i;\ \boldsymbol{\psi}_T,\ T \in \mathscr{T}_h^i\}$. Thus, $\boldsymbol{V}_{h0}^{\mathrm{el}} = \operatorname{span}\{\boldsymbol{\psi}_e,\ e \in \mathscr{E}_h^i;\ \boldsymbol{\psi}_T,\ T \in \mathscr{T}_h^i\}$.

Further, $\dim(\operatorname{span}\{\boldsymbol{\psi}_e,\ e \in \mathscr{E}_h^i;\ \boldsymbol{\psi}_T,\ T \in \mathscr{T}_h^i\}) = \dim(\boldsymbol{V}_{h0}^{\mathrm{el}}) = \dim(\boldsymbol{Z}_{h0}) + \dim(\mathbb{P}_{h0}^0) = \#\mathscr{X}_h^i + \#\mathscr{T}_h^i + \#\mathscr{T}_h - 1 = \#\mathscr{T}_h^i + \#\mathscr{E}_h^i = \#(\{\boldsymbol{\psi}_e,\ e \in \mathscr{E}_h^i;\ \boldsymbol{\psi}_T,\ T \in \mathscr{T}_h^i\})$. Therefore, the functions $\{\boldsymbol{\psi}_e,\ e \in \mathscr{E}_h^i;\ \boldsymbol{\psi}_T,\ T \in \mathscr{T}_h^i\}$ are linearly independent, and they form a basis of $\boldsymbol{V}_{h0}^{\mathrm{el}}$. The proof is completed. □

References

1. Arnold, D.N.: Finite Element Exterior Calculus. SIAM (2018)
2. Arnold, D.N., Falk, R., Winther, R.: Finite element exterior calculus, homological techniques, and applications. Acta Numer. **15**, 1–155 (2006)
3. Arnold, D.N., Qin, J.: Quadratic velocity/linear pressure Stokes elements. In: Advances in Computer Methods for Partial Differential Equations VII, IMACS, 28–34 (1992)
4. Auricchio, F., Beirão da Veiga, L., Lovadina, C., Reali, A.: The importance of the exact satisfaction of the incompressibility constraint in nonlinear elasticity: mixed FEMs versus NURBS-based approximations. Comput. Methods Appl. Mech. Eng. **199**, 314–323 (2010)
5. Auricchio, F., Beirão da Veiga, L., Lovadina, C., Reali, A., Taylor, R.L., Wriggers, P.: Approximation of incompressible large deformation elastic problems: some unresolved issues. Comput. Mech. **52**, 1153–1167 (2013)
6. Boffi, D., Brezzi, F., Fortin, M.: Mixed Finite Element Methods and Applications. Springer, Berlin (2013)
7. Brezzi, F.: On the existence, uniqueness and approximation of saddle-point problems arising from Lagrangian multipliers. R.A.I.R.O. Anal. Numér. **2**, 129–151 (1974)
8. Chen, S., Dong, L., Qiao, Z.: Uniformly convergent $H(\mathrm{div})$-conforming rectangular elements for Darcy-Stokes problem. Sci. China Math. **56**, 2723–2736 (2013)
9. Cockburn, B., Nguyen, N.C., Peraire, J.: A comparison of HDG methods for stokes flow. J. Sci. Comput. **45**, 215–237 (2010)

10. Cockburn, B., Gopalakrishnan, J.: The derivation of hybridizable discontinuous Galerkin methods for Stokes flow SIAM. J. Numer. Anal. **47**, 1092–1125 (2009)
11. Falk, R.S., Morley, M.E.: Equivalence of finite element methods for problems in elasticity. SIAM J. Numer. Anal. **27**, 1486–1505 (1990)
12. Falk, R.S., Neilan, M.: Stokes complexes and the construction of stable finite elements with pointwise mass conservation. SIAM J. Numer. Anal. **51**, 1308–1326 (2013)
13. Gauger, N.R., Linke, A., Schroeder, P.W.: On high-order pressure-robust space discretisations, their advantages for incompressible high Reynolds number generalised Beltrami flows and beyond. SMAI J. Comput. Math. **5**, 89–129 (2019)
14. Guzmán, J., Neilan, M.: A family of nonconforming elements for the Brinkman problem. IMA J. Numer. Anal. **32**, 1484–1508 (2012)
15. Guzmán, J., Neilan, M.: Conforming and divergence-free stokes elements on general triangular meshes. Math. Comput. **83**, 15–36 (2014)
16. Guzmán, J., Neilan, M.: Inf-sup stable finite elements on barycentric refinements producing divergence-free approximations in arbitrary dimensions. SIAM J. Numer. Anal. **56**, 2826–2844 (2018)
17. Guzmán, J., Neilan, M.: Conforming and divergence-free stokes elements in three dimensions. IMA J. Numer. Anal. **34**, 1489–1508 (2013)
18. Hiptmair, R., Li, L., Mao, S., Zheng, W.: A fully divergence-free finite element method for magnetohydrodynamic equations. Math. Models Methods Appl. Sci. **28**, 659–695 (2018)
19. Hu, K., Ma, Y., Xu, J.: Stable finite element methods preserving $\nabla \cdot B = 0$ exactly for MHD models. Numer. Math. **135**, 371–396 (2017)
20. Hu, K., Xu, J.: Structure-preserving finite element methods for stationary MHD models. Math. Comput. **88**, 553–581 (2019)
21. Huang, Y., Zhang, S.: A lowest order divergence-free finite element on rectangular grids. Front. Math. China. **6**, 253–270 (2011)
22. John, V., Linke, A., Merdon, C., Neilan, M., Rebholz, L.G.: On the divergence constraint in mixed finite element methods for incompressible flows. SIAM Rev. **59**, 492–544 (2017)
23. Linke, A., Merdon, C.: Well-balanced discretisation for the compressible Stokes problem by gradient-robustness. In: Finite Volumes for Complex Applications IX - Methods, Theoretical Aspects, Examples, Springer, Cham, 113–121 (2020)
24. Liu, X., Li, J., Chen, Z.: A nonconforming virtual element method for the Stokes problem on general meshes. Comput. Methods Appl. Mech. Eng. **320**, 694–711 (2017)
25. Mardal, K.A., Tai, X.C., Winther, R.: A robust finite element method for Darcy-Stokes flow. SIAM J. Numer. Anal. **40**, 1605–1631 (2002)
26. Neilan, M., Sap, D.: Stokes elements on cubic meshes yielding divergence-free approximations. Calcolo **53**, 263–283 (2016)
27. Nguyen, N.C., Peraire, J., Cockburn, B.: An implicit high-order hybridizable discontinuous Galerkin method for the incompressible Navier-Stokes equations. J. Comput. Phys. **230**, 1147–1170 (2011)
28. Qin, J., Zhang, S.: Stability and approximability of the $P_1 - P_0$ element for Stokes equations. J. Numer. Methods Fluids **54**, 497–515 (2007)
29. Schroeder, P.W., Lube, G.: Divergence-free H(div)-FEM for time-dependent incompressible flows with applications to high Reynolds number vortex dynamics. J. Sci. Comput. **75**, 830–858 (2018)
30. Scott, L.R., Vogelius, M.: Norm estimates for a maximal right inverse of the divergence operator in spaces of piecewise polynomials. RAIRO - Modél. Math. Anal. Numér. **19**, 111–143 (1985)
31. Stenberg, R.: A technique for analysing finite element methods for viscous incompressible flow. J. Numer. Methods Fluids **11**, 935–948 (1990)
32. Tai, X.C., Winther, R.: A discrete de Rham complex with enhanced smoothness. Calcolo **43**, 287–306 (2006)
33. Uchiumi, S.: A viscosity-independent error estimate of a pressure-stabilized Lagrange-Galerkin scheme for the Oseen problem. J. Sci. Comput. **80**, 834–858 (2019)
34. Wang, R., Wang, X., Zhai, Q., Zhang, R.: A weak Galerkin finite element scheme for solving the stationary Stokes equations. J. Comput. Appl. Math. **302**, 171–185 (2016)
35. Xie, X., Xu, J., Xue, G.: Uniformly stable finite element methods for Darcy-Stokes-Brinkman models. J. Comput. Math. **26**, 437–455 (2008)
36. Xu, X., Zhang, S.: A new divergence-free interpolation operator with applications to the Darcy-Stokes-Brinkman equations. SIAM J. Sci. Comput. **32**, 855–874 (2010)
37. Zeng, H., Zhang, C., Zhang, S.: A low-degree strictly conservative finite element method for incompressible flows on general triangulations. SMAI J. Comput. Math, accepted. (2022)
38. Zeng, H., Zhang, C., Zhang, S.: A low-degree strictly conservative finite element method for incompressible flows. arXiv:2103.00705, (2021)

39. Zeng, H., Zhang, C., Zhang, S.: Optimal quadratic element on rectangular grids for H^1 problems. BIT Numer. Math. **61**, 665–689 (2020)
40. Zhang, S.: A new family of stable mixed finite elements for the 3D Stokes equations. Math. Comput. **74**, 543–554 (2005)
41. Zhang, S.: On the P_1 Powell-Sabin divergence-free finite element for the Stokes equations. J. Comput. Math. **26**, 456–470 (2008)
42. Zhang, S.: A family of $Q_{k+1,k} \times Q_{k,k+1}$ divergence-free finite elements on rectangular grids. SIAM J. Numer. Anal. **47**, 2090–2107 (2009)
43. Zhang, S.: Divergence-free finite elements on tetrahedral grids for $k \geq 6$. Math. Comput. **80**, 669–695 (2011)
44. Zhang, S.: Quadratic divergence-free finite elements on Powell-Sabin tetrahedral grids. Calcolo **48**, 211–244 (2011)
45. Zhang, S.: Stable finite element pair for stokes problem and discrete stokes complex on quadrilateral grids. Numer. Math. **133**, 371–408 (2016)
46. Zhang, S.: Minimal consistent finite element space for the biharmonic equation on quadrilateral grids. IMA J. Numer. Anal. **40**, 1390–1406 (2020)
47. Zhang, S.: An optimal piecewise cubic nonconforming finite element scheme for the planar biharmonic equation on general triangulation. Sci. China Math. **64**, 2579–2602 (2021)
48. Zhai, Q., Zhang, R., Wang, X.: A hybridized weak Galerkin finite element scheme for the Stokes equations. Sci. China Math. **58**, 2455–2472 (2015)

Publisher's Note Springer Nature remains neutral with regard to jurisdictional claims in published maps and institutional affiliations.

Springer Nature or its licensor holds exclusive rights to this article under a publishing agreement with the author(s) or other rightsholder(s); author self-archiving of the accepted manuscript version of this article is solely governed by the terms of such publishing agreement and applicable law.